January 2019

Molecular Machinery For The ‘kiss And Run’ Mechanism Of Insulin Secretion

Akshata Ramesh Naik
Wayne State University, akshoo23@gmail.com

MOLECULAR MACHINERY FOR THE 'KISS AND RUN' MECHANISM OF INSULIN SECRETION

by

AKSHATA RAMESH NAIK

DISSERTATION

Submitted to the Graduate School

of Wayne State University,

Detroit, Michigan

in partial fulfillment of the requirements

for the degree of

DOCTOR OF PHILOSOPHY

2019

MAJOR: PHYSIOLOGY

Approved By:

_____

Advisor Date

_____

_____

_____

_____

DEDICATION

I would like to dedicate my thesis to all the wonderful people who have given me constant love and support during the course of my degree and otherwise.

First and foremost, I dedicate this PhD to my parents, the pillars of my life. I have risen to achieve many things by stepping on their shoulders. My mother, Mrs. Chandrika Ramesh Naik, is my very first teacher and my best friend, ever since I can remember. My father, Mr. Ramesh Sampat Naik, has taught me to be strong even in times of extreme difficulties and hardships. Thank you both for the unconditional love and positivity that you create around me.

My brother, Venkatesh R. Naik, to whom, I can pour my heart out. Your determination and sincerity inspires me constantly.

I would also like to dedicate this degree to my in- laws, the ‘Sridhars’ for welcoming me whole- heartedly into their family. Thank you late Mrs. Pushpa Sridhar, my mother-in- law and late Mr. S.V. Sridhar, my father- in- law, for making me one of their own.

Most importantly I would dedicate my PhD to my loving husband and my adorable children.

My husband, Praveen Sridhar is an amazing human being, truly complements me in every way possible. Thank you for reinstating the courage in me each and every time I have needed it. My journey has been mostly smooth and happy because of your presence in my life. You have been wonderful in sharing responsibilities and I know that you are indeed proud of my achievements.

Finally this degree is for none other than my beautiful kids. Whatever I do is because of them and for them. My son, Nischay Sridhar and my daughter, Nivriti Sridhar

are the greatest treasures of my life who make everything else seem tiny.

Additionally, I dedicate this thesis to my maternal grandparents, Smt. Jayalakshmi Srinivasan and Sri. M.A Srinivasan who loved and nurtured me unconditionally.

Thank you everyone for the untiring patience and support expressed towards me during my graduate school journey.

Lastly I would express my gratitude towards the Almighty for guiding me always.

ACKNOWLEDGEMENTS

My boundless gratitude is expressed towards my mentor, Prof. Bhanu P. Jena. It has been my pleasure and honor to be his graduate student. I remember meeting him in his office after enrolling in the PhD program and it has been an upward journey since then. His child- like enthusiasm motivates me to pursue my passion for science. Thank you for your guidance and constructive criticism that has made me the scientist that I am today. My growth in Jena lab has been immensely satisfying in terms of critical thinking, troubleshooting research problems, mentoring undergraduate and master's students, not to mention the enjoyable environment that we all work in.

Along the way, I had the pleasure of working with many other people. Dr. Kenneth T. Lewis, my friend and colleague who taught me during my initial few months of joining this lab. I would like to thank in particular, Dr. Suvra Laha, Mr. Eric Kuhn, Ms. Sanjana Kulkarni and Mr. Nikhil Yedulla, co- authors of chapters in this thesis. I would also like to acknowledge all the wonderful people in the lab, whom I trained and worked with: Dr. Maheshika Pahliwadana, Mr. Keith Kokotovich, Ms. Rishika Pulvender, Mr. Asiri Liyanaraarchi and Mr. Brent Formosa.

I would additionally like to thank my committee members, Dr. Daniel A. Walz, Dr. Joseph C. Dunbar, Dr. Robert J. Wessells and Dr. Christopher V. Kelly for all the advice and suggestions. My gratitude expressed towards the Department of Physiology and its office staff, especially to Ms. Christine Cupps for helping students outside of the lab.

Finally, a big thank you to all my amazing friends – Ken, Carthic, Josh, Eric, Rishika, and Brent, who kept me sane during this degree.

It has been a privilege to work with so many delightful people.

TABLE OF CONTENTS

LIST OF FIGURES

LIST OF ABBREVIATIONS

AFM	Atomic Force Microscopy
EM	Electron Microscopy
MIN6	Mouse Insulinoma Cells
TREK-1	Potassium channel subfamily K member 2 protein
HSP	Heat Shock Proteins
SNARE	Soluble N-ethylmaleimide Sensitive Factor Attachment Protein Receptor
AQP	Aquaporin
ISG	Insulin Secreting Granule
NSF	N-ethylmaleiamide sensitive factor
ATPase	Adenosine Triphosphatse
v H^+ ATPase	vacuolar H^+ ATPase
VPA	Valproate
FDA	Food and Drug Administration
SNAP 25	Synaptosomal Associated Protein 25 kDa
PCS	Photon Correlation Spectroscopy
VAMP	Vesicle Associated Membrane Protein
MIPS	Myo-Inositol Phosphate Synthase
DAG	Diacylglycerol

CHAPTER 1: INTRODUCTION

Cell secretion is a universal phenomenon and is extremely important for a variety of cellular functions. All cells ranging from prokaryotic bacteria, eukaryotic yeasts to mammalian cells undergo secretion[1,2]. A variety of physiological processes such as neurotransmission, release of histamines from mast cells following exposure to allergens, or the release of hormones from endocrine cells to maintain homeostasis all occur from the release of secretory products from within the cells to the cell exterior. These secretory contents are contained within membrane bound compartments termed as 'secretory vesicles' or 'secretory granules'. Upon cell stimulation, secretory vesicles travel to associate with the cell plasma membrane where they dock and fuse at the specialized cup-shaped lipoprotein structures and release their contents to the outside of the cell.

Transient Cell Secretion

Secretion occurs either via complete collapse of the vesicle at the cell plasma membrane, termed as 'total fusion' or via the transient engagement and fusion of the vesicle with the cell plasma membrane, termed as 'kiss-and-run' mechanism[3]. This latter process of kiss-and-run, enabling the release of a portion of intravesicular contents to the outside, while retaining the chemical and morphological integrity of the secretory vesicle following a secretory episode.

The kiss-and-run mechanism of cell secretion is supported by the observation of partially empty vesicles in electron micrographs of cells, following cell secretion. To enable such transient docking and fusion event at the cell plasma membrane, given that vesicle membrane are under high surface tension and therefore would favor collapse at the cell plasma membrane, the presence of a permanent docking and transient fusion

port at the cell plasma membrane was hypothesized and discovered by our laboratory over 20 years ago, and named the 'porosome'[4].

Molecular Machinery for Transient Cell Secretion

Studies now demonstrate that the 'fusion pore', an opening between the vesicle membrane and cell the plasma membrane is established at the porosome base oriented towards the interior of the cell. Historically, the kiss-and-run or transient mode of docking and fusion of secretory vesicles at the cell plasma membrane were proposed in 1973[5,6], which could explain the fractional release of intra-vesicular contents from cells during cell secretion. How this transient mechanism could be accomplished, remained a mystery. Subsequently in 1990, it was suggested that the fusion pore formation, which results from a 'preassembled ion channel-like structure could open and close[6]. In the early 1990s it was proposed that the primary difficulty in observing such preassembled structures at the cell plasma membrane and fusion pore formation at such a level was due to the absence of tools for ultrahigh resolution live cell imaging[7]. The invention of force microscopy in the mid-1980s changed all that. In the mid-1990s, the hypothesis of the presence of secretory portals was confirmed by the discovery of the 'porosome', a new cellular structure at the cell plasma membrane[8] using the atomic force microscope (AFM)[9] an imaging tool that has revolutionized nano-science especially nano cell biology. Using AFM, 100–180 nm in size cup-shaped secretory portals were observed at the plasma membrane of live pancreatic acinar cells that secreted digestive enzymes through them[8]. The presence and morphology of these secretory portals were further confirmed using electron microscopy (EM)[9-11].

Porosomes have been discovered in almost all secretory cells such as neurons,

epithelial airway cells in the lungs, endocrine growth hormone releasing cells of the pituitary gland, and also in endocrine pancreatic beta cells, by our group, and subsequently by other researchers as well[9,12-17]. The function of the porosome as a universal secretory portal, its chemical composition, and its structural and functional reconstitution has been extensively studied and has greatly advanced our understanding of this supra-molecular lipo-protein structure.

Insulin Secreting Porosome Complex

Porosomes in β cells of the endocrine pancreas were demonstrated using EM and AFM on mouse insulinoma (MIN6) cells[18]. The insulin secreting porosome complex range in size, from 100 – 120 nm in diameter, compared to the 15 nm neuronal porosome complex and 100 – 180 nm porosome in pancreatic acinar cells. It is noteworthy, because the size of the porosome complex, correlates well to the size of secretory vesicles, within each cell type. For example, synaptic vesicles ranging in size from 30 – 50 nm[19] dock at porosomes 1/2 to nearly 1/3 the vesicle size while similarly, the insulin secreting granules and zymogen granules measuring on average 500 nm, dock at porosomes measuring nearly 1/3rd the secretory vesicle size (140 nm on average)[20,21]. Structurally, the insulin secreting porosome complex is similar to the acinar cell porosome and it lacks the central plug that is almost exclusive to the neuronal porosome complex for rapid release of neurotransmitters.

Proteome of the Insulin Secreting Porosome Complex

The 100 – 120 nm sized MIN6 cell porosome has been immunoisolated and mass spectrometry reveals that it comprises of approximately 30 different core proteins. On the contrary, the nuclear pore, which is similar in size, is comprised of nearly 1000 protein

molecules[22]. Like any other porosome, the MIN6 cell porosome contains cytoskeletal and motor proteins such as actin, myosin and tubulin. Additionally, membrane channel proteins such as potassium channel subfamily K member 2 protein TREK-1, calcium transporting ATPase are also associated with the MIN6 cell porosome in addition to GTP binding signaling proteins, and heat shock chaperone proteins, HSP70 and HSP90. The presence of these proteins in the MIN6 cell porosome has been further confirmed using immunoisolation and Western Blot[18]. Since HSPs function in both protein folding and in assembly of protein complexes, their presence in MIN6 cell porosome was found to have a similar role. Immunoisolated porosomes from MIN6 cells treated with an inhibitor (17-demethoxy-17-(2-prophenylamino) geldanamycin) against the late chaperone protein, HSP90, involved in protein assembly, exhibited loss of several proteins from the porosome complex[18]. However, the levels of these proteins were unchanged in the total cell homogenate. This strongly suggests that HSP90 is critical to the assembly and folding of the MIN6 porosome complex. It has further been demonstrated that cells exposed to HSP90 inhibitor secrete significantly sub-optimal levels of insulin upon stimulation by glucose.

The MIN6 porosomes also comprise the SNARE (soluble N-ethylmaleimide Sensitive Factor attachment protein receptor) protein, synaptosomal associated protein 25 kDa (SNAP 25). SNAP 25, a target SNARE (t SNARE) protein along with syntaxin 1 interact with vesicular SNARE (v SNARE) proteins such as synaptobrevin to form the multimolecular SNARE complex, important for vesicle fusion at the plasma membrane[23]. When the vesicle membrane and the plasma membrane come in close proximity in the later part of secretion, the t and v SNAREs interact with each other in a circular array and

bring the apposing membranes together to form the fusion pore. The fusion pore thus forms at the base of the porosome complex via t/v SNAREs. It is widely accepted that the bivalent cation Ca^{+2} is involved in bridging, and fusion of the two negatively charged juxtaposed membrane bilayers[24]. It has further been demonstrated, using molecular dynamic simulations that there is expulsion of coordinated water molecule during the membrane lipid mixing process; as hydrated calciums are much bigger (~6 A^{o}) to fit in the space between the opposing bilayers brought together via the t/v SNARE molecular complex (~2.8 A^{o})[25]. The distance between the membrane bilayers held together by calcium phosphate bridges is demonstrated to be 2.92 A^{o}[25].

Apart from carrying the secretory products and anchoring v SNARE proteins in its membrane facing the cell cytosol, the secretory vesicle has a greater role to play in the process of secretion. The vesicle itself is a microcosm of biochemical signaling cascade, harboring many molecules such as ion and water channels along with signaling proteins such as heterotrimeric G proteins in its membrane, that are involved in the regulation of vesicle volume required for the expulsion of vesicular contents.

The physiology of the secretory vesicle with regards to its volume and pH are critical for cell secretion. Swelling of granules prior to release was suggested as early as the 1960s and was thereafter confirmed as a requirement for mast cell degranulation[26]. Secretory vesicle swelling provides increase in membrane surface tension for vesicle fusion with the plasma membrane and osmotic gradient for vesicular content release following the establishment of continuity between the porosome membrane.[27] Hence, preventing secretory granule swelling has been demonstrated to compromise secretion competency[28]. This swelling phenomenon has been confirmed in secretory vesicles of

various cell types such as zymogen granules of acinar cells of exocrine pancreas and synaptic vesicles of neurons. The bidirectional water channel, aquaporins (AQP) are involved in rapid gating of water molecules into the granules and are regulated by the GTPase activity of G proteins present at the secretory granule membrane[29-31]. It has further been demonstrated in neuronal synaptic vesicles that swelling is pH sensitive. Preventing acidification of synaptic vesicles lowers vesicle volume even after GTP stimulation[32]. Thus, the pH of secretory granules, play a critical role in regulating vesicle physiology, and consequently, cell secretion.

This study is aimed at further understanding the role of the 3 main components of transient kiss-and-run secretion machinery in cells elaborated previously, namely involvement of the porosome, SNARE protein complex and the insulin secretory granules (ISG).

Specific Aims

Specific Aim I: Functional reconstitution of the insulin secreting porosome complex in live cells.

The neuronal porosomes and the acinar cell porosomes have been immunoisolated and both structurally and functionally reconstituted into artificial lipid bilayers. Both of these types of porosomes have been characterized structurally and functionally using AFM, EM, solution x-ray, mass spectrometry and electrophysiological apparatus respectively[10,12]. However, the insulin secreting porosome complex from MIN6 cells had not been studied. Given the importance of insulin secretion in physiology, further characterization of the insulin-secreting porosome complex in beta cells and its functional reconstitution into live cells was investigated. To study using a homogenous beta cell population, rat insulinoma MIN6 cells[18] were used throughout the study.

Specific Aim II: Intravesicular and intracellular pH is critical for glucose stimulated insulin release.

Secretory vesicles maintain a relatively lower pH compared to the cell cytoplasm, which is important for vesicle homeostasis[33]. In this study, we have confirmed these results in insulin secreting MIN6 cells demonstrating that blocking pH drop pharmacologically, significantly reduces glucose stimulated insulin release.

Specific Aim III: Assembly and disassembly of SNARE protein complex is pH dependent.

Once the SNARE complex is formed allowing for vesicle docking on to the plasma membrane, it has to be disassembled to terminate the secretion process. A protein termed as N-ethylmaleiamide sensitive factor (NSF) enables disassembly of SNARE complex[34]. NSF is an ATPase associated with several cellular activities, making it an AAA+ ATPase[35]. Although NSF is ubiquitously found in the cell cytoplasm, we hypothesized that its ATPase activity is sensitive to changes in intracellular pH.

Specific Aim IV: Identification of an epileptic drug that affects glucose stimulated insulin secretion.

The ISG contains the proton pump vacuolar H+ ATPase (vH^+ ATPase) on the granule membrane. Valproate, an FDA approved anticonvulsant is used in the treatment of epileptic seizures. Although specific mechanistic actions of the drug are unknown, it is highly suggested that the main target of valproate is the vH^+ ATPase pump[36]. The proton pump is also present on neuronal synaptic vesicles, thereby regulating neurotransmitter release[37]. Our study was involved in understanding the mechanism of action of this drug on MIN6 cells and its effects on the proton pump.

CHAPTER 2: FUNCTIONAL RECONSTITUTION OF THE INSULIN SECRETING POROSOME COMPLEX IN LIVE CELLS

(This Chapter contains previously published material. See Appendix A)

Abstract

Supramolecular cup-shaped lipoprotein structures called porosomes embedded in the cell plasma membrane mediate fractional release of intravesicular contents from cells during secretion. The presence of porosomes, have been well documented in many cell types that include neurons, acinar cells of the exocrine pancreas, growth hormone secreting cells of the pituitary, and insulin-secreting pancreatic beta cells, and functionally reconstituted into artificial lipid membrane. Earlier studies on mouse insulin-secreting MIN6 cells report 100 nm porosome complexes composed of nearly 30 proteins. In the current study, porosomes have been functionally reconstituted for the first time in live cells. Isolated MIN6 porosomes reconstituted into live MIN6 cells demonstrated augmented levels of porosome proteins and a consequent increase in the potency and efficacy of glucose-stimulated insulin release. Elevated glucose-stimulated insulin secretion 48h post reconstitution, reflects on the remarkable stability and viability of reconstituted porosomes, documenting the functional reconstitution of native porosomes in live cells. These results, establish a new paradigm in porosome-mediated insulin secretion in beta cells.

Introduction

Glucose stimulated release of insulin stored in secretory vesicles in β cells occur either by complete collapse of the vesicle membrane at the cell plasma membrane, or the transient fusion of secretory vesicles at the base of plasma membrane associated 100 nm cup-shaped lipoprotein structures composed on nearly 30 proteins, called

porosomes[18,38]. Porosomes mediate fractional release of intravesicular contents during cell secretion and consequently in electron micrographs, partially empty secretory vesicles accumulate in cells following a secretory episode[4]. In earlier studies, isolated porosomes from the exocrine pancreas and neurons have been structurally and functionally reconstituted into artificial lipid membranes[10,12]. Transmission electron micrographs of pancreatic porosomes reconstituted into PC: PS liposomes, exhibit a 150 – 200 nm cup-shaped basket-like morphology, similar to its native structure in cells[10]. Similarly, isolated neuronal porosomes reconstituted into lipid membrane appear nearly identical to the native structure at the presynaptic membrane[10,12]. In these earlier studies, the functionality of isolated porosomes obtained from the exocrine pancreas and neurons have been tested following their reconstitution into lipid membrane of an electrophysiological bilayer apparatus EPC9. Membrane-reconstituted porosomes on exposure to isolated secretory vesicle preparations in the presence of calcium exhibit an increase in conductance and capacitance, demonstrating the fusion of the isolated secretory vesicles at the porosome-reconstituted lipid bilayer and the consequent intra-vesicular content release. Furthermore, in the presence of various modulators of porosome proteins, altered fusion and release is observed, demonstrating the isolated porosome complexes to be functional.

The current study on MIN6 cells using electron microscopy (EM), atomic force microscopy (AFM), and immuno-AFM, demonstrate as previously reported in MIN6 cells[18], partially empty docked vesicles at the base of 100 nm cup-shaped porosomes at the cell plasma, through which insulin is released. Photon correlation spectroscopy (PCS) on isolated porosomes from MIN6 cells, demonstrate them to measure on an average

100 nm. To test whether isolated porosomes from MIN6 cells can be functionally reconstituted into live MIN6 cells, and to determine their stability and viability following cellular reconstitution, the current study was undertaken. Results from this study demonstrate that isolated MIN6 porosomes reconstituted into live MIN6 cells exhibit an increase in potency and efficacy of glucose-stimulated insulin release within one hour following reconstitution and sustained even 48h later. This is the first demonstration of the functional reconstitution of porosomes in a live cell, documenting the establishment of a new paradigm in porosome-mediated insulin secretion.

Experimental Procedures

MIN6 Cell Culture

MIN6 mouse insulinoma cells were cultured according to published procedure[18] in high-glucose (25 mM) Dulbecco's Modified Eagle Medium (DMEM) (Invitrogen) supplemented with 10% fetal calf serum, 50 μM β-mercaptoethanol and antibotics (Penicillin and Streptomycin). Porosome isolations and electron microscopy were performed using MIN6 cells grown to confluence in 100 x 13 mm sterile plastic petri dishes. Immunofluorescence microscopy was performed on MIN6 cells grown to 60-70% confluence in 35 mm petri dishes with glass bottom coverslips (MatTek, Ashland, MA).

Electron Microscopy

Transmission electron microscopy of MIN6 cells was performed as described in a previously published procedure[17,39]. Briefly, cells were fixed in 2% glutaraldehyde/ 2% paraformaldehyde in ice-cold PBS for 24 h, washed with buffer, embedded in 2% SeaPrep agarose, followed by post-fixation for 1 h at 4 □C using 1% OsO4 in 0.1 M cacodylate buffer. The sample was then dehydrated in a graded series of ethanols,

through propylene oxide, and infiltrated and embedded in Spurr's resin. Ultrathin sections were cut with a diamond knife, retrieved onto 200 mesh nickel thin-bar grids, and contrasted with alcoholic uranyl acetate and lead citrate. Grids were viewed with a JEOL 1400 transmission electron microscope (JEOL USA, Inc., Peabody, MA) operating at 60 or 80 kV, and digital images were acquired with an AMT-XR611 11 megapixel CCD camera (Advanced Microscopy Techniques, Danvers, MA).

Atomic Force Microscopy

AFM was performed according to minor modification of previously published procedure[8,9,16,40], on fixed (2% glutaraldehyde/ 2% paraformaldehyde) MIN6 cells grown on glass cover slips. Fixed cells in phosphate buffered saline or PBS (1X) pH 7.4, were incubated for 30 min at R.T. in insulin antibodies at a final concentration of 0.2□g/ml (Santa Cruz Biotechnology Inc, Santa Cruz, CA), followed by 30 min incubation in 30 nm-Gold conjugated secondary antibody (experimental). Control experiments were performed by exposing fixed MIN6 cells to secondary Gold conjugated antibody, followed by fixation, prior to imaging using the AFM. Imaging was performed using the Nanoscope IIIa AFM from Digital Instruments. (Santa Barbara, CA). Images were acquired in the "tapping" mode in air, using silicon nitride tips with a spring constant of 0.38 N.m-1, and an imaging force of <200 pN. Images were obtained at line frequencies of 2 Hz, with 512 lines per image, and constant image gains. Topographical dimensions of cellular structures were analyzed using the software nanoscope IIIa4.43r8, supplied by Digital Instruments.

Insulin-Secreting Porosome Isolation and Reconstitution

SNAP-25 specific antibody conjugated to protein A-sepharose® was utilized to

immunoisolate the porosome complex from solubilized MIN6 cells. The solubilization buffer was composed of 2% Triton X-100, 1 mM benzamidine, 5 mM Mg-ATP, and 5 mM EDTA in PBS at pH 7.4, supplemented with protease inhibitor mix (Sigma, St. Louis, MO). Each immunoisolation utilized 2 mg of Triton-solubilized control MIN6 cells. Five micrograms of SNAP-25 antibody conjugated to the protein A-sepharose® were incubated with the 2 mg of the solubilized cells for 1 h on ice, followed by three washes of 10 volumes of wash buffer (500 mM NaCl, 10 mM Tris, 2 mM EDTA, pH 7.5). The immuno pull down complex associated with the immunosepharose beads was eluted using low pH (pH 3.0) PBS (1X) to dissociate the porosome complex from the antibody bound to the beads, and the eluted sample was immediately returned to neutral pH in a total volume of 200 µL. An 80 µL of the isolated porosome suspension and 100 µL of 1 mg/ml of solubilized MIN6 homogenates were aliquoted and resuspended in Laemmli reducing sample preparation buffer[41], boiled for 2 min, and used for SDS-PAGE and Western blot analysis. 100 µL of the isolated porosome preparation was added to a confluent MIN6 cell culture grown in a 100 x 13 mm sterile plastic petri dish[42] to enable reconstitution.

Glucose-Stimulated Insulin Secreting from MIN6 Cells

MIN6 cells grown to confluence in 100 x 13 mm sterile plastic petri dishes, and following 30 min exposure to isolated pososomes, were monitored for glucose-stimulated insulin release at 1h to 48h following porosome reconstitution. All secretion assays were performed at room temperature (25 □C). Cells were washed three times using 5ml/wash of PBS, pH 7.4, and incubated in 35 mM glucose-PBS. 200 µL aliquots were removed at times 0, 10, and 30 min following 35 mM glucose incubation. The aliquots were

centrifuged at 4,000 x g to remove any cells that may have been aspirated, and 160 µL of the supernatant was mixed with 40 µL of 5x Laemmli reducing sample preparation buffer[41], boiled for 2 min, and resolved using SDS-PAGE followed by Western blot analysis utilizing a insulin-specific antibody. Following completion of the secretion assays, cells were solubilized in equal volumes of PBS, their protein concentration determined. To compare total insulin in the control and reconstituted cells, equal volume of the cell lysate in Laemmli reducing sample preparation buffer[41] was immunoblotted using insulin-specific antibodies. 5 µg of the cell lysate was also used in SDS-PAGE and Western blot analysis to determine the immunoreactive presence of various porosome-associated proteins. Percent insulin release was measured from the optical densities of insulin Western blots of the secreted and whole cell lysates.

Western Blot Analysis

Isolated MIN6 homogenates and porosomes in Laemmli buffer were resolved in a 12.5% SDS-PAGE, followed by electrotransfer to 0.2 mm nitrocellulose membrane. The membrane was incubated for 1h at room temperature in blocking buffer (5% nonfat milk in phosphate buffered saline or PBS (1X) pH 7.4 containing 0.1% Triton X-100 and 0.02% NaN3) and immunoblotted for 2 h at room temperature with antibodies raised against insulin (Santa Cruz Biotechnology Inc, Santa Cruz, CA), and porosome associated proteins Gαi3, Syntaxin-1A, and TREK-1 (K+ channel) (Santa Cruz Biotechnology Inc, Santa Cruz, CA), all at a final concentration of 0.2 μg/ml in blocking buffer. The immunoblotted nitrocellulose sheets were washed in PBS (pH 7.4) containing 0.1% Tween, prior to incubation for 1h at room temperature in horseradish peroxidase-conjugated secondary antibodies at a dilution of 1:5000 in blocking buffer. The

immunoblots were washed in PBS containing 0.1% Tween and processed for enhanced chemiluminescence and exposure to X-Omat-AR film. The exposed films were then developed and photographed.

Immunofluorescence Microscopy

To determine the distribution of the porosome-associated protein Gαi3 and SNAP-25 in control and porosome-reconstituted MIN6 cells, immunofluorescence studies were performed according to published procedures[17]. To determine the position of the cell nucleus, cells were exposed to DAPI nuclear stain (Molecular Probes, Life Technologies, Carlsbad, CA). Phase and immunofluorescent images were acquired using an immunofluorescence FSX100 Olympus microscope through a 100x objective lens (numerical aperture = 1.40) with illumination at 405 nm, 488 nm, or 647 nm. The co-association of Gαi3 and SNAP-25 and their cellular distribution was determined by merging the fluorescent and phase images.

Results and Discussion

Atomic force microscopy (AFM), transmission electron microscopy (TEM), and small angle X-ray solution scattering (SAXS) studies, combined with electrophysiology, biochemistry, and molecular biology approaches, have played a major role in the discovery of the porosome –the universal secretory portal in cells, and determination of its nanometer-scale structure-function in a variety of cell types including β-cells of the endocrine pancreas[38] and in mouse insulinoma MIN6 cells[18]. The porosome was discovered nearly two decades ago, first in acinar cells of the exocrine pancreas[8,10], and subsequently in chromaffin cells of the adrenal medulla[43], growth hormone GH-secreting cells of the pituitary, at the terminals of neurons[12,39,42], in astrocytes[15], in hair cells of the

inner ear[44], and in various cell lines such as the rat basophilic cell line RBL-2H3, the human bone marrow mononuclear cells BMMC[45], in the mucin-secreting Calu-3 cells of the human airways epithelia[44], and in the insulin-secreting MIN6 cells[17], amongst others. In the current study, both EM and AFM were used to further study the morphology of MIN6 cells and the porosomes associated at its cell plasma membrane. Transmission EM and AFM performed on fixed MIN6 cells demonstrate the presence of typically 100 - 300 nm membrane bound secretory vesicles, and the presence of approximately 100 nm porosomes (Figure 2.1). In EM micrographs, the 100 nm cup-shaped porosomes are also found with docked secretory vesicles (Figure 2.1 A [b]). The morphology of coated pits (Figure 2.1 A [c]) in comparison, are much different from the porosome structures. While porosomes in MIN6 cells have a cup-shaped morphology, coated pits appear nearly spherical with a thick coat (Figure 2.1 A [c]). Photon correlation spectroscopy (PCS) of the isolated MIN6 porosomes, also demonstrate an average size of approximately 91 nm (Figure 2.1 A [d]), similar to what is observed in the electron micrographs (Figure 2.1 A [b])[17]. AFM studies of insulin-immuno gold-labeled MIN6 cells demonstrate the localization of immunogold to the porosome opening (Figure 2.1 B [f]), which is absent in porosomes of control MIN6 cells, which had been exposed only to the secondary gold-conjugated antibody (Figure 2.1 B [d,e]). Similar to earlier immuno-AFM studies on the exocrine pancreas[9,10] and the growth hormone secreting cells[16] of the pituitary gland, the immunolocalization of insulin-immunogold at the porosome opening (Figure 2.1 B [f]), and the presence of partially empty docked secretory vesicles at the porosome base (Figure 2.1 A[b]), demonstrates the 100 nm cup-shaped structures at the cell plasma membrane of MIN6 cells to be the secretory portals for fractional release of intravesicular insulin

during cell secretion.

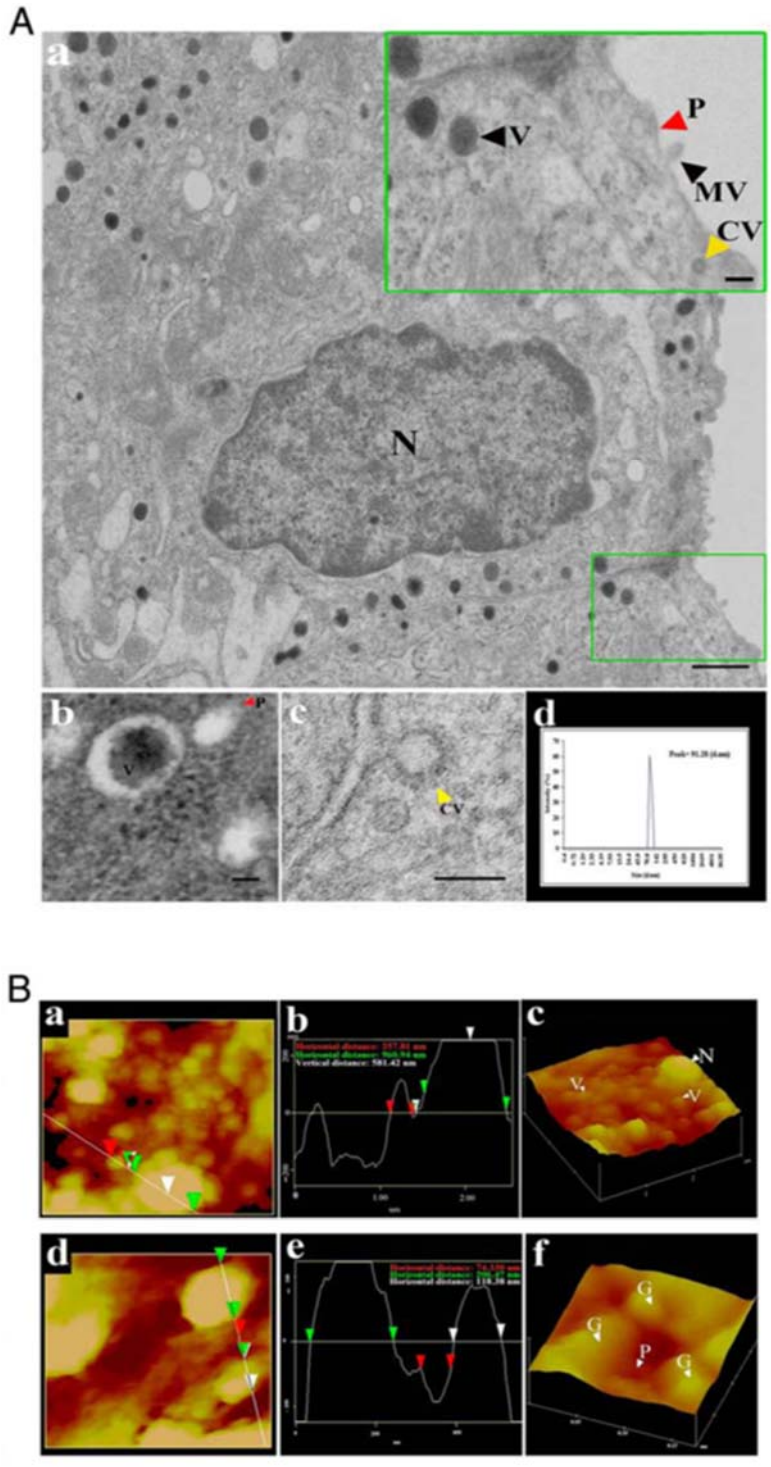

Figure 2.1: Electron and atomic force micrographs of MIN6 cells demonstrate the presence of cup-shaped porosome complexes at the cell plasma membrane. (A[a]) Electron micrograph of a MIN6 cell, and the nucleus (N), insulin containing electron dense secretory vesicles (V), mitochondria (M), porosome (P), coated vesicle (CV), and microvilli (MV), within the cell. Scale bar = 500 nm. (A[b]) Two 100 nm porosomes at the cell plasma membrane, one with a docked secretory vesicle that has a portion of its contents released. (A[c]) A coated vesicle at the MIN6 cell plasma membrane, illustrating the shape and size difference compared to the porosome. (A[d]) Photon correlation spectroscopy of isolated MIN6 porosome complex demonstrates its average size to measure approximately 91 nm. (B[a]) Two-dimensional atomic force microscope image of a portion of MIN6 cell, demonstrating the nucleus size, and size-heterogeneity between insulin-containing vesicles. (B[b]) Section analysis demonstrates the secretory vesicle to measure 258 nm. (B[a]) Low surface distance, compared to the nucleus measuring 961 nm in surface distance and 581 nm in height (B[b]). In (B[c]), a three-dimension AFM image of (B[a]) is shown for clarity. (B[d]) High-resolution two-dimensional atomic force micrograph of a portion of Min6 cell, demonstrating the presence of the nucleus to the top left, two secretory vesicles to the right and a porosome between the two. (B[e]) Section analysis of this control MIN6 cells exposed to 30 nm-Gold conjugated secondary, demonstrates the presence of secretory vesicles measuring 232 nm and 437 nm. The porosome opening measures 136 nm, and no gold particles are observed at the site. (B[f]) Three-dimensional atomic force microscope image of a Min6 porosome (P) with several 30 nm immuno gold (G) particles localized at the porosome opening.

Isolated MIN6 Porosomes Reconstitute into Live MIN6 Cells

Porosomes from MIN6 cells were isolated using antibody directed at the porosome-associated t-SNARE protein SNAP25 and immuno pull down. The isolated MIN6 porosomes were reconstituted into live MIN6 cells by incubating MIN6 cells in culture with the immunoisolated MIN6 porosomes for various periods. Porosome reconstitution was evaluated using Western blot analysis and immunocytochemistry. The functional reconstitution of porosomes into live MIN6 cells was also determined by measuring the potency and efficacy of glucose-stimulated insulin secretion at 1 h, 24 h, and 48 h following porosome reconstitution, and compared to insulin release from control MIN6 cells.

Immunoisolated porosomes from MIN6 cells when subjected to mass spectrometry[17] demonstrated the presence of approximately 30 core proteins, among them SNAP-25, Gαi3, Syntaxin-1A, and TREK-1. Western blot analysis on equal protein amounts of total cellular homogenates from control and porosome-reconstituted MIN6 cells demonstrated that the porosome associated proteins Gαi3, Syntaxin-1A, and TREK-1, are elevated in the reconstituted cell homogenate fraction (Figure 2.2 A). No change in insulin immunoreactivity is observed in the reconstituted MIN6 cell homogenates, demonstrating that porosome reconstitution has no influence on the total amount of cellular insulin. To further confirm porosome reconstitution in MIN6 cells, immunocytochemistry using Gαi3 and SNAP-25 primary antibody, followed by secondary fluorescent rhodamine and fluorescene antibodies respectively, were utilized. Elevated level of the co-localized presence of Gαi3 and SNAP-25 is observed in the porosome-exposed MIN6 cells (Figure 2.2 B [a] over 2.2 B [b]), demonstrating porosome

reconstitution (Figure 2.2 B). To further demonstrate porosome reconstitution in live MIN6 cells, a functional assessment of glucose-stimulated insulin secretion following reconstitution was required, and was performed in the study.

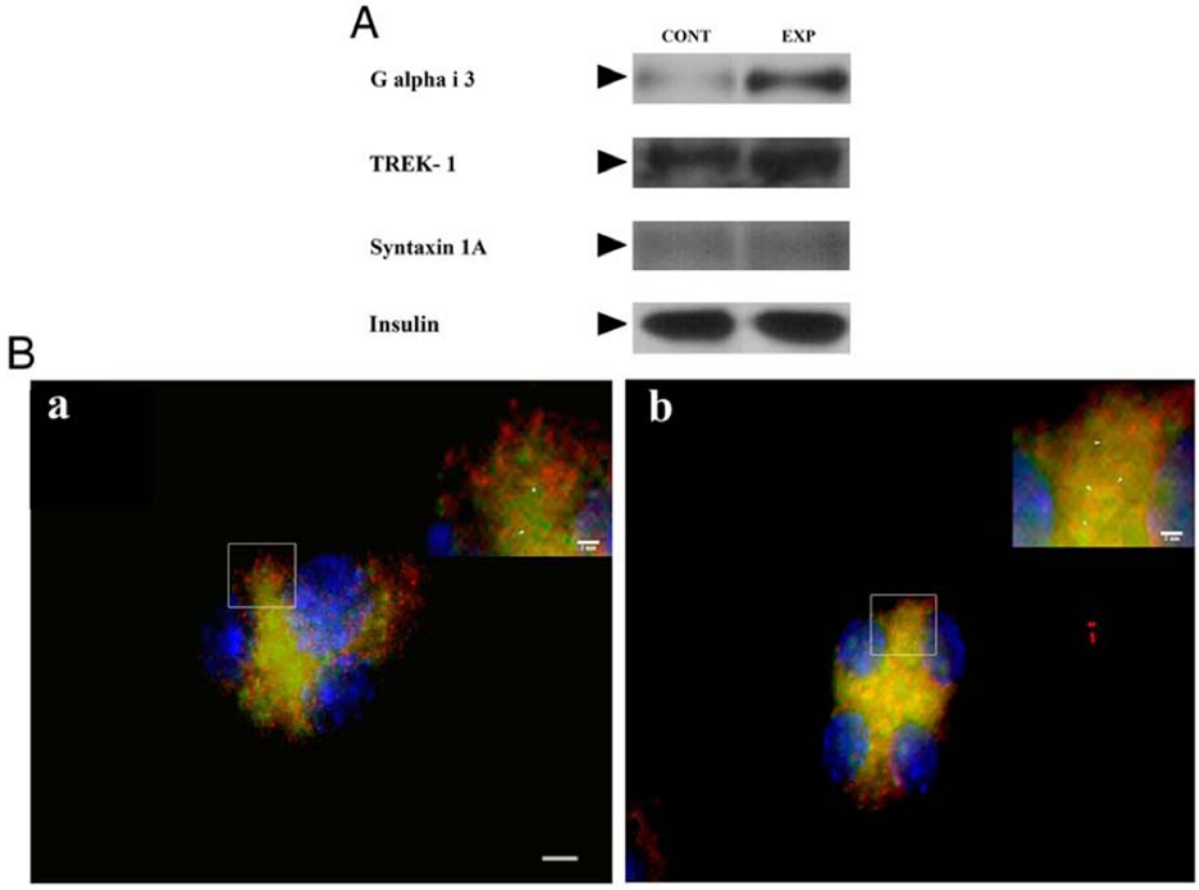

Figure 2.2: Enriched presence of TREK-1, Gαi3, and Syntaxin-1A immunoreactivity in porosome-reconstituted MIN6 cells. (A) Western blot analysis of 5 µg of MIN6 cell homogenate from control and porosome-reconstituted cells. Note the enriched presence of all three porosome proteins: TREK-1, G□i3, and Syntaxin-1A. No change in insulin immunoreactivity is observed in the reconstituted MIN6 cell homogenate. (B) Immunofluorescence microscopy demonstrates increased Syntaxin-1A and G□i3 immunoreactivity and their increased co-localized presence in porosome-reconstituted MIN6 cells.

Reconstituted Cells Exhibit Increased Glucose-Stimulated Insulin Release

To test whether the porosome complexes reconstituted into live MIN6 cells are functional, glucose-stimulated insulin release assays were carried out on both control and porosome-reconstituted MIN6 cells. A time-dependent increase in insulin release is

observed in both control, and porosome-reconstituted MIN6 cells upon exposure to glucose (Figure 2.3 A, B). Although little change in the basal levels of insulin release is observed in MIN6 cells 1h following reconstitution with the porosome complex, a significant ($p<0.05$) increase in glucose-stimulated insulin secretion is demonstrated in the reconstituted cells 30 min following exposure to elevated glucose over controls (Figure 2.3 B). In addition to demonstrating an increase in the potency of insulin secretion,

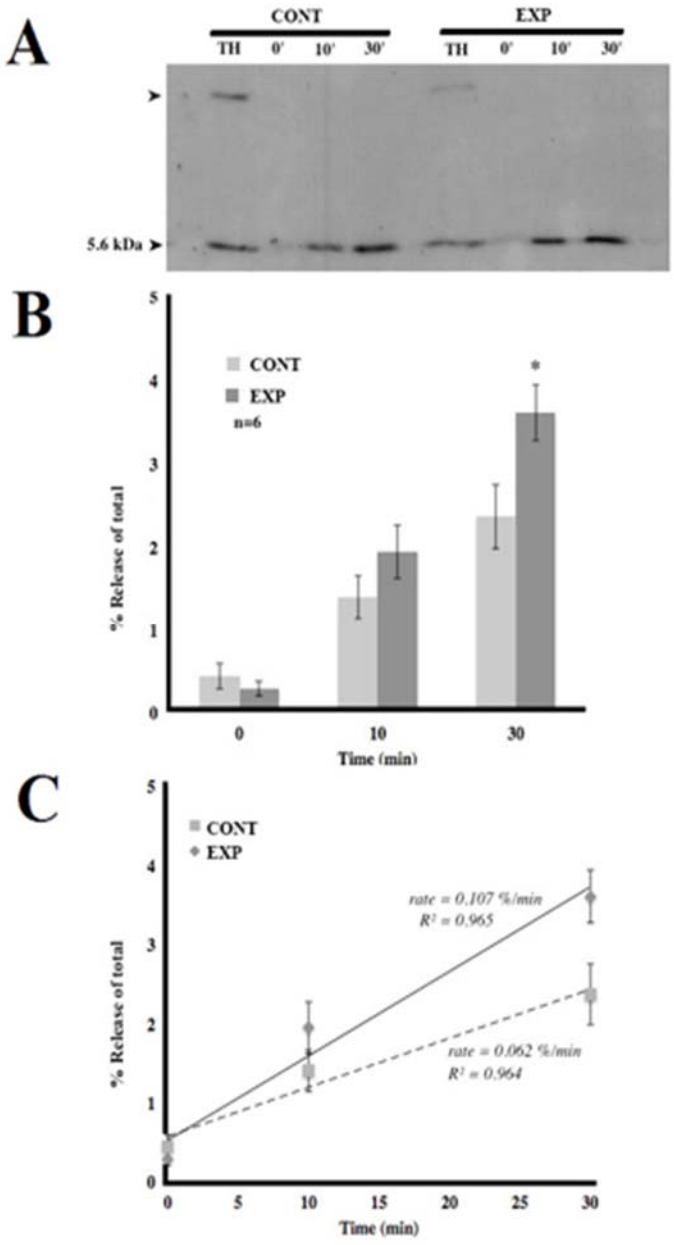

Figure 2.3: Porosome-reconstituted MIN6 cells demonstrate elevated glucose-stimulated insulin secretion. Note the increase in time-dependent insulin release from reconstituted MIN6 cells. (A) Representative insulin immunoblot of total MIN6 cell homogenate (TH) and glucose-stimulated insulin release at times 0, 10, and 30 min, in control and porosome-reconstituted experimental MIN6 cells. A preproinsulin band is present only in the total homogenate fraction and not in the secreted fraction. (B) Bar graph of percent insulin release at time 0, 10, and 30 min, in control and reconstituted experimental MIN6 cells. A significant increase in time-dependent insulin release from porosome-reconstituted MIN6 cells is observed in the 30 min time point (n=6; *$p < 0.05$). Note, no change in basal insulin release is observed in porosome-reconstituted MIN6 cells. (C) The rate of insulin secretion per minute was calculated to be 0.062%/min of the total in control cells that increased to 0.107%/min of the total in the porosome-reconstituted cells, a 70% increase in the insulin release rate.

porosome-reconstitution results in >70% increase (from 0.062%/min to 0.107%/min) in the efficacy of glucose-stimulated insulin release in MIN6 cells (Figure 2.3 C). These results demonstrate for the first time, the functional reconstitution of isolated insulin-secreting porosomes into live insulin secreting MIN6 cells, and the consequent increase in both the potency and efficacy of insulin release. The observed time-dependent increase in insulin secretion, and the presence of proinsulin in the total homogenate (TH) fractions (Figure 2.3 A) from both control and experimental (reconstituted) MIN6 cells, and its absence in the secreted fraction in both groups, demonstrate the MIN6 cells to be intact and viable. Next, we determined the stability of reconstituted porosomes into live cells, to understand the life span of porosome complexes in cells for possible future therapeutic applications.

Porosome Reconstitution is Stable and Functional

To determine the stability of reconstituted porosomes in live MIN6 cells, the elevated presence of porosome associated proteins Gαi3, Syntaxin-1A, and TREK-1, in porosome-reconstituted MIN6 cells, and their glucose stimulated insulin secretion was assessed 24 h and 48 h following reconstitution.

Similar to results obtained at the 1h time point following porosome reconstitution, there are elevated levels of Gαi3, Syntaxin-1A, and TREK-1, in porosome-reconstituted MIN6 cell homogenates (Figure 2.4 A). Results from this study further demonstrates sustained glucose stimulated insulin secretion at both 24 h and 48 h following porosome reconstitution (Figure 2.4 B). Similar to results obtained at the 1 h time point following porosome reconstitution, there is little change in the basal levels of insulin secretion, however the elevated glucose stimulated insulin secretion is continually maintained in the

reconstituted cells, demonstrating the functional stability of the reconstituted porosome complex.

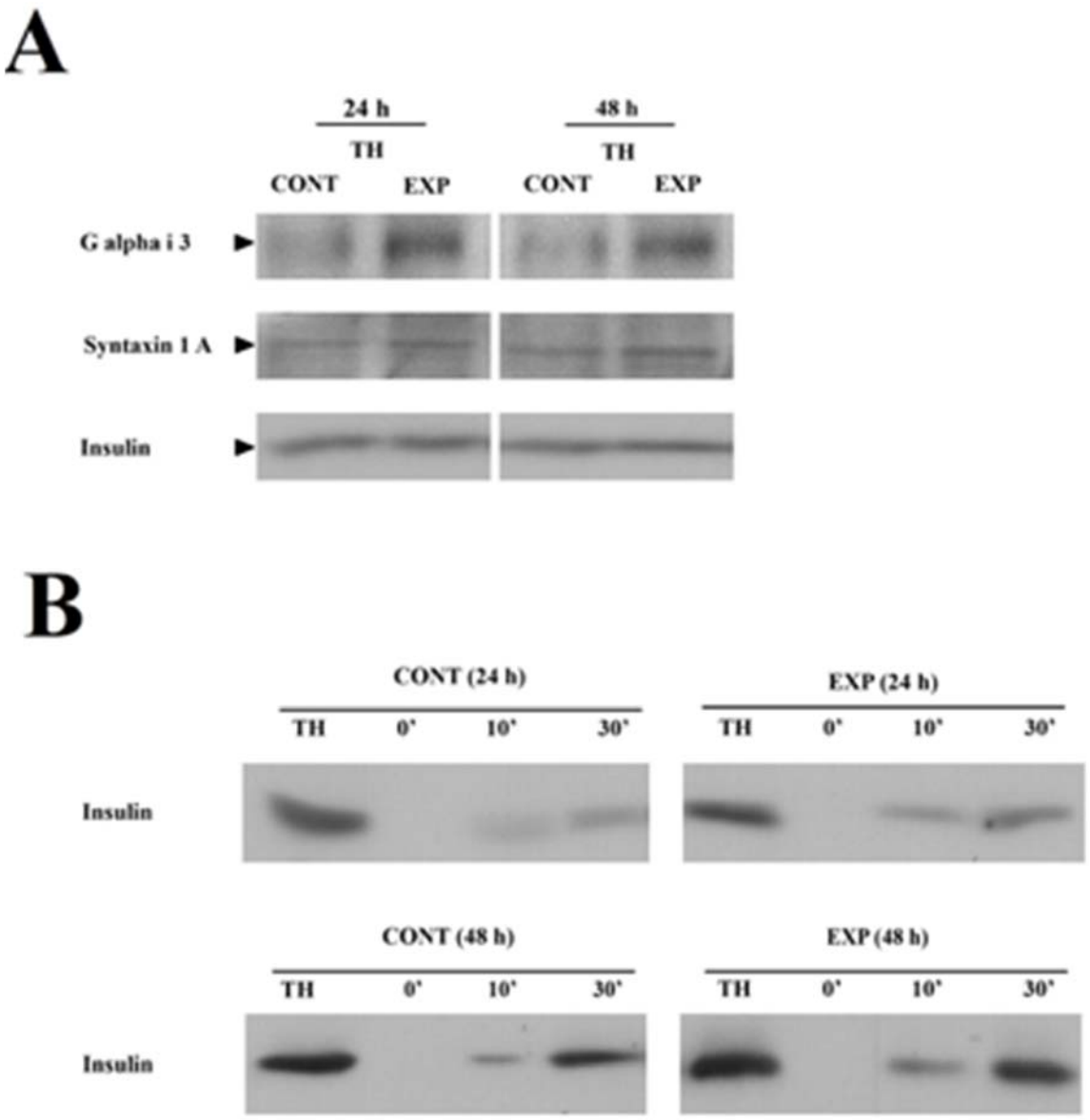

Figure 2.4: Enriched presence of TREK-1, Gαi3, and Syntaxin-1A immunoreactivity in homogenates of porosome-reconstituted MIN6 cells, and the consequent glucose-stimulated insulin release is observed at 24h and 48h following reconstitution. (A) Representative Western blots of MIN6 cell homogenate from control and porosome-reconstituted (experimental) MIN6 cells at 24h and 48h, demonstrating the enriched presence of the porosome proteins TREK-1, Gαi3, and Syntaxin-1A. No change in total insulin immunoreactivity is detected in the experimental homogenate. (B) The enriched presence of porosome proteins in (A), is reflected on the elevated levels of glucose-stimulated insulin release in both the 24h and 48h following porosome reconstitution into MIN6 cells.

In conclusion, this is the first demonstration of the functional reconstitution of isolated porosomes in live cells. Reconstitution of porosomes isolated from the exocrine pancreas[9] and neurons[12], into artificial lipid membrane, have previously been reported. In the current study, isolated insulin-secreting porosomes from MIN6 cells have been successfully reconstituted in live MIN6 cells, demonstrating that the isolated insulin-secreting porosome complex is functionally intact. Results from this study further establish the role of porosome as a universal secretory portal in cells, which regulates the kiss-and-run mechanism of fractional insulin release[46]. In further agreement with the porosome-mediated kiss-and-run mechanism of cell secretion, it has been demonstrated that “secretory granules are recaptured largely intact following stimulated exocytosis in cultured endocrine cells”[47]; “single synaptic vesicles fuse transiently and successively without loss of identity”[48]; and “zymogen granule exocytosis is characterized by long fusion pore openings and preservation of vesicle lipid identity”[49]. Utilizing the porosome-mediated kiss-and-run mechanism of secretion in cells, secretory vesicles are capable of reuse for subsequent rounds of exo-endocytosis, until completely empty of contents.

CHAPTER 3: INTRAVESICULAR AND INTRACELLULAR pH IS CRITICAL FOR GLUCOSE STIMULATED INSULIN RELEASE

Abstract

Swelling of secretory vesicles is critical to cell secretion as shown previously in synaptic vesicles of neurons. The heterotrimeric G protein mediated synaptic vesicle swelling occurs via water gating aquaporin channels. Water follows into the vesicles after proton (H^+ ions) entry through vacuolar H^+ ATPase (vH^+ ATPase) pump. In insulin secreting MIN6 cells, we show that insulin granule acidification occurs primarily via vH^+ ATPase since use of bafilomycin A prevents granule acidification. Furthermore, granule acidification plays an important role in glucose stimulated insulin secretion as bafilomycin A treatment prevents insulin secretion in MIN6 cells. Additionally, we demonstrated accumulation of insulin granules upon bafilomycin A treatment as shown by immunocytochemistry.

Introduction

The secretory vesicles apart from acting as cargo tightly regulate the exocytosis of release products. The internal volume of secretory vesicle is important for optimum secretion. Osmotic swelling of granules were first suggested and demonstrated in sea urchin eggs[50,51]. Further it was proved in mast cells that osmotic swelling of granule is important for fusion of secretory vesicle with the plasma membrane in addition to fusion pore dilation[52]. Henceforth, importance of vesicle swelling in fusion and exocytosis was determined in a variety of different granules such as zymogen granules of pancreatic acinar cells, and synaptic vesicles of the neuron to name a few[29,53]. The extent of vesicle swelling is shown to be directly proportional to the amount content released out of the cell[53].

The molecular mechanisms underlying the swelling process have been fairly elucidated. Aquaporins (AQP), the rapidly gating water channels are present on the secretory granule membrane of acinar zymogen granules, synaptic vesicles of rat brain, intracellular vesicles of rat kidney and mouse liver[31,54,55] and are involved in causing osmotic swelling of vesicles. At least 13 different isoforms of aquaporins have been identified; AQP1 is present on the zymogen granules while AQP6 is present on the synaptic vesicles. The aquaporins are under the control of heterotrimeric G proteins, more specifically $G_{\alpha i}3$ in zymogen granules and $G_{\alpha o}$ in the neuronal synaptic vesicles. Although the exact mechanisms have not yet been deduced, the electrochemical gradient generated by the influx of protons (H^+ ions) are a major drive in the events that follow to increase vesicle volume. The proton pump, vacuolar H+ ATPase (vH^+ ATPase) present on the synaptic vesicle membrane operates upstream of $G_{\alpha o}$ induced aquaporin mediated synaptic vesicle swelling[32].

The heterotrimeric G protein, $G_{\alpha i}$ is localized on the insulin secretory granules and it stimulates insulin secretion[56]. If insulin secreting cells follow a similar pathway of modifying granule physiology then lower granular pH is of prime importance. Additionally, the acidic pH of intragranular lumen is also important for conversion of insulin from its prohormone and maturation of the granule[57-59].

In this study, we used MIN6 cells and subjected them to Bafilomycin A, a pharmacological inhibitor of vH^+ ATPase thus preventing acidification of the cell and insulin secreting granules (ISG). We demonstrated a significant loss in glucose stimulated insulin secretion in the treated cells as compared to the controls. Additionally we showed an accumulation of insulin within the Bafilomycin A treated cells. Theoretically, we could

isolate the insulin granules and perform experiments to monitor live changes in volume and pH. But, insulin granules are highly unstable and lyse instantaneously.

Experimental Procedures

Glucose Stimulated Insulin Secretions from MIN6 Cells in Culture

MIN6 cells were grown to confluence using sterile 100 X 13-mm plastic Petri dishes according to published procedure[60]. Cells were cultured in 25 mM glucose Dulbecco's Modified Eagle Medium (Invitrogen) containing 10% fetal calf serum, penicillin, streptomycin, and 50μM B-mercaptoethanol. Cells were stimulated using 35 mM glucose, and insulin secreted into the medium was collected at 10 and 30 min. Stimulation assays were performed 10min after exposure to 10nM and 50nM Bafilomycin A respectively. All secretion assays were carried out at room temperature (RT), and the cells were washed with phosphate buffered saline (PBS) pH 7.4 prior to stimulation. Following glucose stimulation, 200 μL aliquots of the supernatants were collected at 0, 10 and 30 min post stimulation. Aliquots were centrifuged at 4000 X g to remove any aspirated cells, and 160 μL of the supernatant was mixed with 40 μL of 5x Laemmli reducing sample preparation buffer[41] for Western blot assay. To obtain the total amount of insulin in cells, Min6 cells were solubilized in 100 μL of homogenization butter (2 mM EDTA, 2 mM ATP, 0.02% Triton X-100, 1:500 protease inhibitor cocktail, pH7.4) following secretion assays, and protein concentrations[61] were determined prior to Western blot analysis.

Detection of Intracellular and Intragranular pH Changes in MIN6 Cells

MIN6 cells were cultured on 35 mm glass bottom petri dishes and were treated with either 10 nM Bafilomycin A, 50 nM Bafilomycin A or with vehicle. Changes in intracellular and intragranular pH were detected using acridine orange (AO). AO is a

membrane penetrating dye, which is a weak base that accumulates within acidic compartments of the cell. AO emits a bright orange fluorescence at lower pH shifting to dimmer orange at relatively basic pH. MIN6 cells were incubated with AO (2 µg/ mL) for 20 minutes at 37° C post treatment with Bafilomycin A or vehicle, washed with sterile 1x PBS, pH 7.4. Orange compartments indicating acidic granules were observed under fluorescence microscopy.

Western Blot Analysis

MIN6 cell lysates (10 µg) in Laemmli buffer were resolved on 12.5% SDS-PAGE and electro-transferred to 0.2 mm nitrocellulose membrane. The membrane was incubated at RT for 1 h in blocking buffer (5% non-fat milk in PBS- 0.1% Tween pH 7.4), washed thrice with PBS-0.1% Tween, and immunoblotted at 4□C overnight with mouse polyclonal anti-insulin (2D11-H5) (SC 8033). Prior to incubation for overnight at 4°C with secondary antibodies (Donkey anti-Rabbit Alexafluor 594 (Invitrogen A21207) nitrocellulose membranes were washed in PBS-0.1% Tween pH 7.4, thrice. Immunoblots were processed for enhanced chemiluminescence, exposed to X-Omat-AR film, developed and analyzed using ImageJ.

Immunocytochemistry

MIN6 cells were grown on 35 mm glass bottom Petri dishes for immunocytochemistry. The distribution of anti- $G\alpha_{i3}$ subunit and ISGs in 10nM and 50nM Bafilomycin A treated (10min at 37°C) MIN6 cells were compared with vehicle treated control MIN6 cells. Primary antibodies, rabbit polyclonal anti- $G\alpha_{i3}$ (SC 262) and mouse polyclonal anti-insulin (SC 8033) and secondary antibodies, Donkey anti-Rabbit Alexafluor 594 (Invitrogen A21207) and donkey anti-Mouse Alexafluor 488 (Life

technologies A21202), were used in the study. Cells were exposed to DAPI nuclear stain for nucleus localization. An immunofluorescence FSX100 Olympus microscope was used to acquire immunofluorescent images through a 63x objective lens (numerical aperture, 1.40) with illumination at 405, 488, or 647 nn. Insulin and $G\alpha_{i3}$ localization and cellular distribution were obtained through merging fluorescent images using ImageJ.

Results and Discussion

Bafilomycin A Prevents Acidification of Insulin Granules

Bafilomycin A and concanamycins are a related family of pleicomacrolide antibiotics derived from Streptomycetes species. They are highly specific pharmacological inhibitors of vacuolar H^+ ATPase (vH^+ ATPase) without affecting any other type of ATPase pump[62,63].

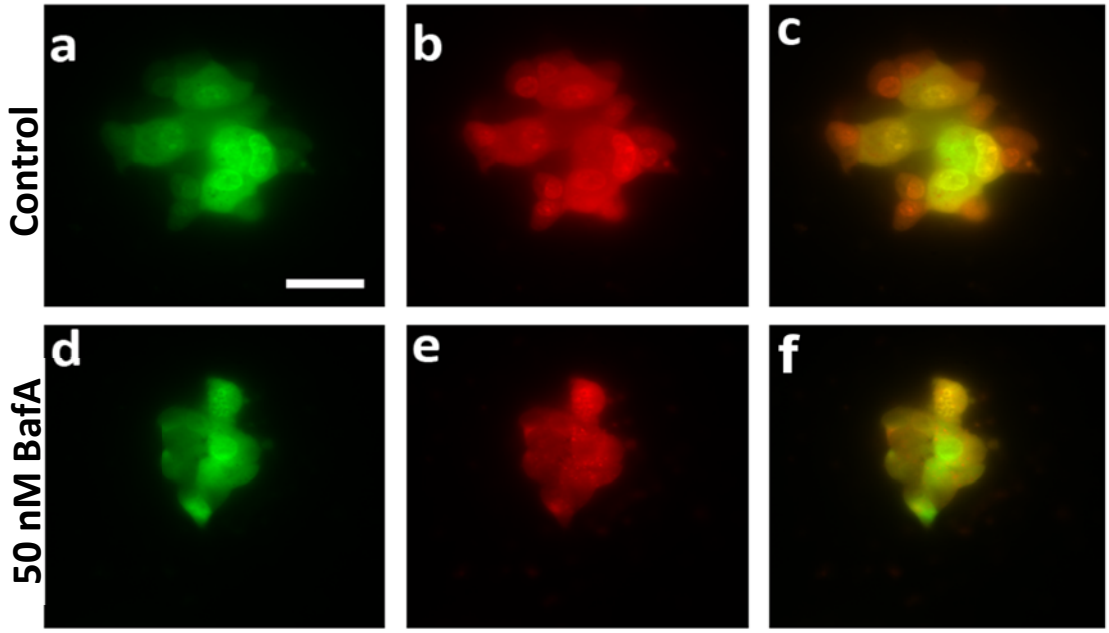

Figure 3.1: **Bafilomycin A inhibits intragranular acidification in MIN6 cells.** MIN6 cells were incubated with 50nm Bafilomycin A for 10 minutes at 37°C and loaded with acridine orange. Note the drop in bright orange fluorescence in treated cells (f) as compared to control cells (c). *Scale bar* = 50 μm.

MIN6 cells were incubated with acridine orange (AO), which accumulated within intracellular compartments. These intracellular compartments have a high probability of

being insulin secreting granules since majority of the cell interior is made up of granules. Bright orange fluorescence was observed within control MIN6 cells depicting acidified granules (Figure 3.1, a-c). MIN6 cells pretreated with 50 nm Bafilomycin A exhibited a quenched fluorescence, not being as bright as the control cells (Figure 3.1, d-f). Hence, this concludes that Bafilomycin A was able to inhibit acidification of secretory granules within MIN6 cells.

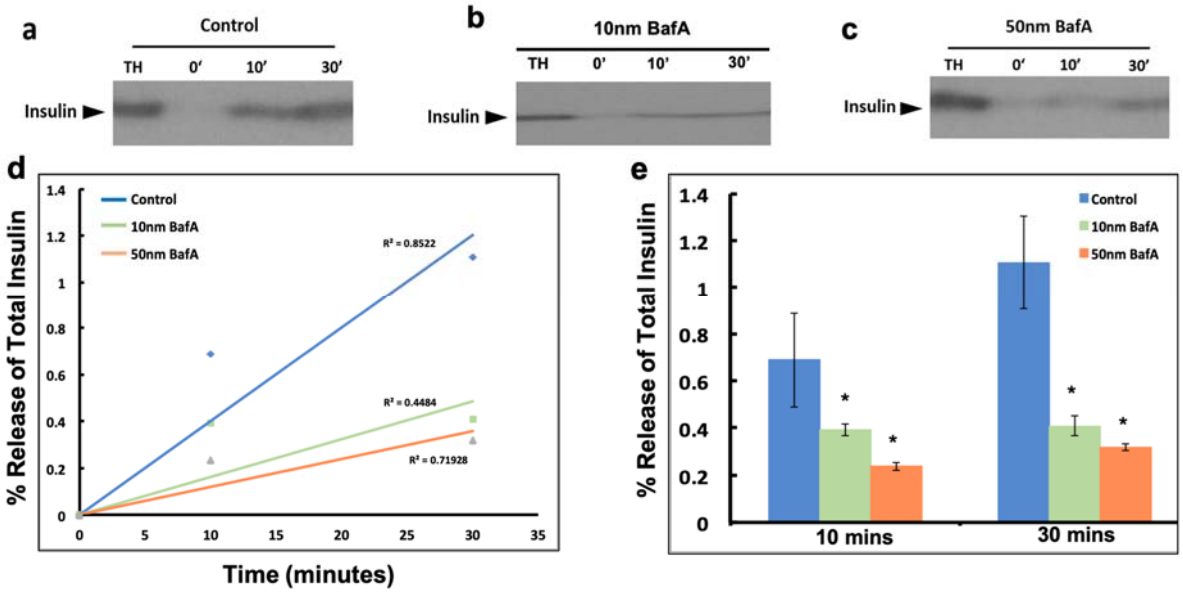

Figure 3.2: Bafilomycin A reduces glucose stimulated insulin release in MIN6 cells. Both 10 nM and 50 nM (c) Bafilomycin A significantly decreases insulin secretion at 10 and 30 minutes post glucose stimulation as depicted in western blots compared to controls (a). Additionally, bafilomycin A reduces the rate of insulin release (d) and also the amount of insulin released (e); *$p < 0.05$, $n = 3$.

Bafilomycin A Treatment of MIN6 Cells Inhibit Glucose Stimulated Insulin Secretion

The importance of pH in granule maturation is well established[64]. Therefore, we wanted to test whether Bafilomycin A treatment has an effect on glucose stimulated insulin secretion. We observed a significant reduction ($p < 0.05$) in insulin secretion upon Bafilomycin A treatment of MIN6 cells. Both, 10 nM and 50 nM Bafilomycin A showed statistically much lower insulin release compared to vehicle treated controls (Figure 3.2). Not just the potency, but also the efficacy of glucose stimulated insulin release was

reduced in the Bafilomycin A treated MIN6 cells (Figure 3.2, d,e).

Bafilomycin A Treatment Reduces Insulin Granule Association with the Plasma Membrane

Immunocytochemistry was performed on control and Bafilomycin A treated MIN6 cells. Antibody against insulin was used to depict insulin secreting granules as insulin is contained inside granules within the cells. Additionally, antibody against $G_{\alpha i}3$ was used as a membrane marker since the heterotrimeric G protein is a transmembrane protein. MIN6 cells treated with 10 nM and 50 nM Bafilomycin A demonstrated reduced co-localization of insulin secreting granules with $G_{\alpha i}3$ as opposed to the control cells which showed more co-localization (Figure 3.3, a-l).

Additionally, the density of insulin antibody is significantly highest in both the 10 nM and 50 nM Bafilomycin A treated MIN6 cells as compared to controls (Figure 3.3, m). This suggests that there is a high probability of ISG accumulation within the treated MIN6 cells that are not being secreted out.

Therefore, these set of results demonstrate that ISG acidification is critical for insulin release. When granule acidification was prevented using bafilomycin A, insulin release dropped dramatically. The events that follow insulin granule acidification are important and can be studied as a future direction. In neuronal synaptic vesicles, vesicle swelling after water entry via AQP has been demonstrated. MIN6 ISG could follow a similar pathway since ISG swelling is also critical for insulin release. Similarly, the signaling events upstream of ISG acidification are yet to be elucidated completely. It is extremely difficult for ISGs to survive *in vitro*, outside of the cell. Hence this limits monitoring *in vitro* ISG swelling and analyzing their surface charge using photon correlation spectroscopy.

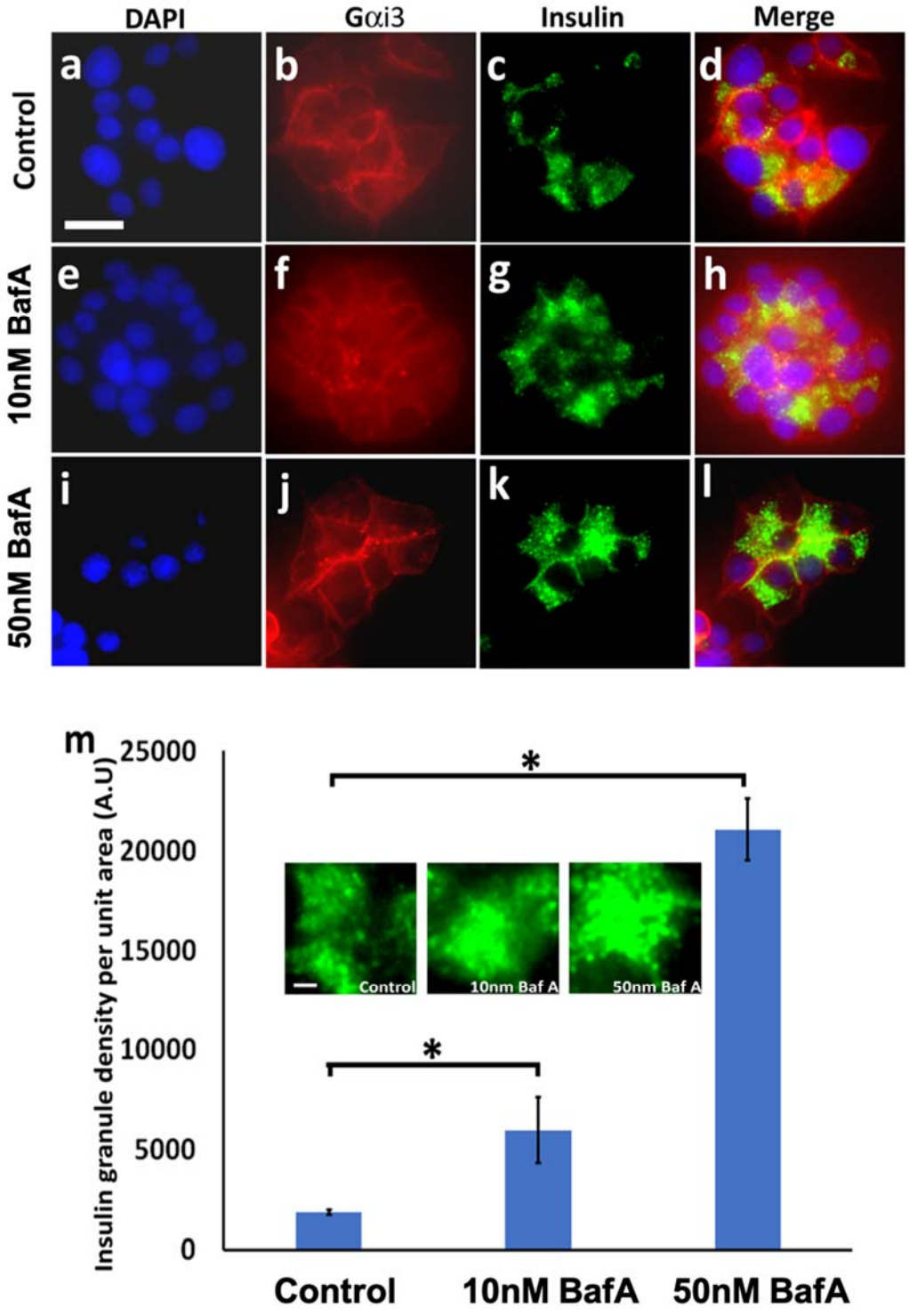

Figure 3.3: Bafilomycin treatment leads to accumulation of insulin within MIN6 cells. Notice increase in insulin granules (green) in 10 nm Bafilomycin A (h) and 50 nm Bafilomycin A (l) treated cells compared to control cells (d). Scale bar = 100 μm. Imagej analysis demonstrates significantly higher antigen density of insulin granules in treated cells as compared to controls (m); *$p < 0.05$. Insets depict digitally zoomed regions of equal areas if insulin (green) channel to show ISG accumulation within control, 10 nm and 50 nm Bafilomycin A treated cells.

Since vH^+ ATPase are the primary ion channels that help reduce ISG pH, understanding the working molecular mechanisms of vH^+ ATPase is useful as well. vH^+ ATPase is a multimolecular subunit with each subunit having a specific function that is important for insulin release. However, further research awaits in understanding the role of ISG physiology critical for insulin release.

CHAPTER 4: ASSEMBLY AND DISASSEMBLY OF SNARE PROTEIN COMPLEX IS PH DEPENDENT

(This Chapter contains previously published material. See Appendix B)

Abstract

Intracellular pH homeostasis governs a variety of cellular activities such as protein folding and cell secretion including neurotransmission and insulin release. Nanoscale pH measurements of cells and biomolecules therefore hold great promise in understanding a plethora of cellular functions, in addition to disease detection and therapy. An unusual approach using cadmium telluride quantum dots (CdTeQDs) as fluorescent pH sensors, combined with imaging, spectrofluorimetry, atomic force microscopy, and Western blot analysis, enabled us to study intracellular pH dynamics regulating cell secretion. This tool provided us with highly precise relative pH measurements during insulin secretion. Additionally, the pH-dependent interaction between membrane fusion proteins, also called the soluble N-ethylmaleimide Sensitive Factor activating protein receptor (SNARE), was determined. CdTeQD-loaded insulin secreting MIN6 cells demonstrated an initial (5-6 min) intracellular acidification upon glucose stimulation, which was reflected as a loss in QD fluorescence, followed by alkalization and a return to resting pH in 10 min. Analysis of the SNARE complex in insulin secreting MIN6 cells demonstrated a consequent increase initially followed by loss of complexed SNAREs within 10 min. Further, using both, native and recombinant neuronal SNAREs, we confirmed that relatively lower pH stabilizes the SNARE complex, providing a molecular understanding of the role of intracellular pH during cell secretion.

Introduction

There has been tremendous improvement in obtaining accurate pH measurements

of cells and biomolecules over the years[65]. However, we still face major challenges at the nanometer and milli-pH scale in cells. Nano scale and single molecule intracellular measurements of pH hold great promise in understanding an array of cellular functions at the molecular level and for applications from disease detection to therapy[65]. Cellular phenomenon such as autophagy and mitophagy alter intracellular pH[66], in addition to a number of diseases; among them cancer and Alzheimer's[67,68]. Intracellular alkalization is shown to inhibit cell secretion,[69,70] whereas acidification stimulates release[71,72]. The role of intracellular acidification in SNARE protein complex assembly/ disassembly is poorly understood, and is the subject of the current study. Secretion from cells involves fusion of cargo containing membrane bound vesicles with the cell plasma membrane. Specialized membrane fusion proteins at the vesicle membrane called v-SNARE[73], and at the cell plasma membrane termed target or t-SNAREs interact and assemble in a t-/v-SNARE rosette or ring conformation to promote fusion between opposing lipid membranes[74,75]. The t-/v-SNARE is a very stable complex, requiring an ATPase called N-ethylmaleimide-sensitive factor (NSF) for its disassembly. The ATPase activity of NSF requires basic pH optima[76,77]. To determine the time-dependent shifts in intracellular pH following stimulation of cell secretion, fluorescent-stable pH-sensitive 2 nm cadmium telluride quantum dots (CdTeQDs) were used[78,79], as opposed to the commonly used pH-sensitive fluorescent dyes such as (2',7'-Bis-(2-Carboxyethyl)-5-(and-6)-Carboxyfluorescein Acetoxymethyl Ester) (BCECF) and Acridine Orange (AO) that bleaches rapidly upon exposure to light.

In this study, intracellular pH dynamics during cell secretion was determined utilizing MIN6 cells, a well-characterized glucose-sensitive insulin-secreting mouse

insulinoma sourced cell line that accurately models the pancreatic beta cell[60]. Additionally, MIN6 cells and immunoisolated SNARE complexes from rat brain neurons were both used, to determine the effects of pH on assembly-disassembly states of native SNAREs. Further, recombinant neuronal SNARE proteins expressed in E. coli, affinity purified and reconstituted into artificial liposomes, were used to further establish SNARE assembly-disassembly in different pH environments *ex vivo*.

Experimental Procedures

Estimation of Cellular pH Changes by Quantum Dots, Following Stimulation of Secretion

The relative fluorescent intensities of CdTeQDs were estimated at different pH, using a Hitachi F-2000 Fluorescence spectrophotometer. 5 µL of CdTeQDs (5mg/mL) was resuspended in 2.5 mL of PBS (1X) (1:500) with pH intervals ranging from 4.1 to 10.3. Then 500 µL of the resuspended QDs were added to a cuvette to measure their fluorescent intensities. The excitation wavelength was kept fixed at λex=350nm for these COOH functionalized CdTe core-type QDs (Sigma-Aldrich) with emission at λem=520nm. Changes in intracellular pH following stimulation of secretion, was assessed by preloading MIN6 cells with CdTeQDs, followed by glucose exposure. 150 µg/mL of 2 nm CdTeQDs was added to a MIN6 cell suspension in DMEM-HG growth media (Dulbecco's Modified Eagle Medium (GE Healthcare), 25 mM glucose, 10% fetal calf serum, 50 µM β-mercaptoethanol, 100 U/mL Penicillin, and 100 µg/mL Streptomycin). After 45 minutes of incubation, the cells were washed and resuspended in PBS pH 7.4. Cells were then imaged using an optical microscope (Zeiss; Axiovert 200, Plan-Apochromat 100x/1.40 oil DIC, Axiocam r.1.2 color, Axiovision Rel. 4.8), before and following addition of 35 mM glucose. Images were captured at 1 minute intervals before and immediately following

glucose exposure. The fluorescent intensity of images obtained were analyzed and graphed using the Origin 8.5 software. Further confirmation of intracellular pH change after stimulation was measured in suspended cells by fluorescence spectrophotometry. 10 mL of MIN6 cells in suspension were centrifuged at 200 x g and resuspended in 110 µL containing 1.5 mg/ml CdTeQDs and incubated for 15 minutes on ice. After incubation, CdTeQD-treated cells were diluted 95x in PBS and added to a quartz cuvette. After 2 minutes of equilibration in the chamber, measurements were made every 2 seconds for 720 seconds, with 35 mM glucose added for stimulation at the 120 seconds time point. The first 120 seconds of measurements were averaged and used to calculate the baseline relative signal for the post glucose stimulation time points.

MIN6 Cell Culture

MIN6 mouse insulinoma cells were cultured according to published procedure in DMEM-HG[60]. Fluorescence microscopy was performed on MIN6 cells grown to 60-70% confluence in 35 mm petri dishes with glass bottom coverslips (MatTek, Ashland, MA).

Expression and Isolation of Full-Length Neuronal T-SNARES, V-SNARE and NSF

-terminal xHis-tag constructs for SNAP-25 and NSF, C-terminal 6xHis-tag constructs for Syntaxin 1A and VAMP2 were generated according to published procedures. All four proteins were expressed with 6xHis at full length in E. coli (BL21DE3) and isolated by Ni-NTA (nickel-nitrilotriacetic acid) affinity chromatography (Qiagen, Valencia, CA) as previously published[80]. Protein concentration was determined by BCA assay.

Preparation of Proteoliposomes

All lipids were obtained from Avanti Polar Lipids (Alabaster, AL). A 5 mM lipid stock

solution was prepared by mixing lipid solution in chloroform-DOPC (1,2-dioleoyl phosphatidylcholine): DOPS (1,2-dioleoyl phosphatidylserine) in 70:30 mol/mol ratios in glass test tubes. The lipid mixture was dried under gentle stream of nitrogen and resuspended in 5 mM sodium phosphate buffer, pH 7.5, by vortexing for 5 minutes at room temperature. Unilamellar vesicles were formed following sonication for 2 minutes, followed by a 50 nm pore size extruder. Vesicles ranging in size from 42 - 62 nm in diameter were obtained as assessed by AFM and photon correlation spectroscopy (PCS). Two sets of proteoliposomes were prepared by gently mixing either t-SNARE complex (Syntaxin-1/SNAP-25; final concentration 25 μM) or VAMP2-His6 (final concentration 25 μM) with liposomes[80,81], followed by three freeze/thaw cycles to enhance protein reconstitution at the vesicles membrane.

Atomic Force Microscopy

Atomic force microscopy (AFM) was performed on liposomes placed on mica surface in buffer, using a minor modification of our previously published procedure[75,81]. Liposomes were imaged using the Nanoscope IIIa AFM from Digital Instruments. (Santa Barbara, CA). Images were obtained in the “tapping” mode, using silicon nitride tips with a spring constant of 0.38 N.m-1, and an imaging force of <200 pN. Images were obtained at line frequencies of 2 Hz, with 512 lines per image, and constant image gains. Topographical dimensions of the lipid vesicles were analyzed using the software nanoscope IIIa4.43r8, supplied by Digital Instruments.

Measurement of Liposome (PC:PS Vesicles +/- T-SNARE and V-SNARE) Size Using Photon Correlation Spectroscopy (PCS)

Size of liposomes, proteoliposomes, and proteoliposome clusters were determined using PCS. PCS is a well-known technique for the measurement of size of μm to nm size

particles and macromolecules. PCS measurements were performed in a Zetasizer Nano ZS, (Malvern Instruments, UK). The size distributions of bare PC: PS vesicles and vesicle-reconstituted SNAREs were determined using built-in software provided by Malvern Instruments. Prior to determination of the vesicle hydrodynamic radius, calibration of the instrument was performed using latex spheres of known size. In PCS, subtle fluctuations in the sample scattering intensity are correlated across microsecond time scales. The correlation function was calculated, from which the diffusion coefficient was determined using the Stokes-Einstein equation, hydrodynamics radius can be acquired from the diffusion coefficient[82]. The intensity size distribution, which was obtained as a plot of the relative intensity of light scattered by particles in various size classes, was then calculated from a correlation function using built-in software. The particle scattering intensity is proportional to the molecular weight squared. Volume distribution can be derived from the intensity distribution using Mie theory[83]. The transforms of the PCS intensity distribution to volume distributions can be obtained using the provided software by Malvern Instruments.

Immunoisolation of the Native T-/V-SNARE-NSF Complex and Immunoblot Analysis of NSF Associated with the Complex

To isolate the neuronal t-/v-SNARE-NSF complex and associated proteins, SNAP-25 specific antibody (Santa Cruz, goat, 33 µg/mL, sc-7538) conjugated to protein A-sepharose® was used. 10 mg of whole rat brain solubilized in Triton/Lubrol solubilization buffer (0.5% Lubrol; 1 mM benzamidine; 5 mM Mg-ATP; 5 mM EDTA; 0.5% Triton X-100, in PBS pH 7.4) supplemented with protease inhibitor mix (Sigma, St. Louis, MO), was used for the immunoisolation of the complex. Protein was estimated by the Bradford method[61]. SNAP-25 antibody conjugated to the protein A- sepharose® was incubated

with 1 mg of the solubilized fractions for 1 h at 4°C followed by three washes of 10 volumes of PBS pH 7.4. Washed beads were centrifuged at 500 x g for 2 minutes after each wash and the supernatant was discarded. The immunoisolatated sample attached to the immunosepharose beads was split equally into four parts, and each part suspended and incubated at room temperature or 30 sec in either pH 7.4 +/- ATP, or in pH 6.0 +/- ATP. Following the 30 seconds incubation at room temperature, the immunosepharose beads were isolated and Laemmli sample preparation buffer was added to them. The unboiled protein samples in Laemmli buffer were then resolved using a 10% SDS-PAGE. Following electrotransfer to a 0.2 mm thick nitrocellulose membrane, the resolved proteins underwent immunoblot analysis using specific primary antibodies to NSF (Santa Cruz, goat, 200 ng/ml, sc-15915, lot#C012), syntaxin-1A (Santa Cruz, mouse, 200 ng/ml, sc-12736, lot#D0617), and insulin (Santa Cruz, rabbit, 20 ng/ml, sc-9168, lot#J0615) and HRP-conjugated secondary antibodies for goat (Santa Cruz, donkey, 80 ng/ml, sc-2020, lot#J0614), rabbit (Santa Cruz, doneky, 80 ng/ml, sc-2313, lot#H1806), and mouse (Santa Cruz, donkey, 80 ng/ml, sc-2314, lot#A3114). Western blotting of membranes was carried out according to a previously published protocol (29). Student's t-test was performed on percent change over control on densitometric scan intensities of the NSF immunobands, for comparison between groups with significance established at $P<0.01$(*).

T/V SNARE Complex Analysis on MIN6 Cells Homogenate at Various Time Intervals

MIN6 cells were grown to confluence in 100 x 13 mm sterile plastic Petri dishes according to previously published procedure[60]. Assays were performed at room temperature (25 ^{o}C). Briefly, MIN6 cells were divided into three sets and each set was

stimulated with glucose for different time periods. Cells were washed thrice with 5 mL/wash of PBS (pH 7.4) and exposed to 35mM glucose either for 1 minute, 5 minutes or 10 minutes. After every time point, cells were solubilized in equal volumes of PBS and their protein concentrations were determined. 10 µG of the cell homogenate in Laemmli reducing sample preparation buffer[41] was used in 10% SDS-PAGE and Western blot analysis to determine the status of the SNARE complex at various intervals post glucose exposure. Immunoblot analysis of MIN6 cell homogenates electrotransferred on 0.2mm thick nitrocellulose membrane was performed using primary antibodies specific to syntaxin-1A (Santa Cruz, mouse, 200 ng/ml, sc-12736, lot#D0617), and insulin (Santa Cruz, rabbit, 20 ng/mL, sc-9168, lot#J0615) and HRP-conjugated secondary antibodies for rabbit (Santa Cruz, doneky, 80 ng/mL, sc-2313, lot#H1806), and mouse (Santa Cruz, donkey, 80 ng/ml, sc-2314, lot#A3114).

Results and Discussion

A sensitive intracellular pH detection system was required to test our hypothesis on intracellular pH dynamics upon stimulation of cell secretion. This was accomplished by utilizing core-type -COOH functionalized hydrophilic CdTeQDs, with λex = 350nm and λem = 520nm. Quantum dots are highly resistant to photo-bleaching, and their fluorescence intensity depends on its surrounding pH, allowing accurate pH detection over minutes. Obtaining such measurements are extremely challenging by instantly photo-bleaching pH sensitive dyes[78]. CdTeQDs sized approximately 2 nm were used for cellular analysis following *ex vivo* characterization of their fluorescence intensities in PBS suspensions of varying pH (Figure. 4.1 a). A relatively acidic PBS suspension elicited a diminished intensity of green fluorescence from the CdTeQDs (Figure. 4.1 a). Moreover,

the fluorescent signal to pH curve was highly linear be-tween pH 6.0 - 7.0 and pH 7.0 - 9.0 favoring accurate interpolation in the cellular pH range.

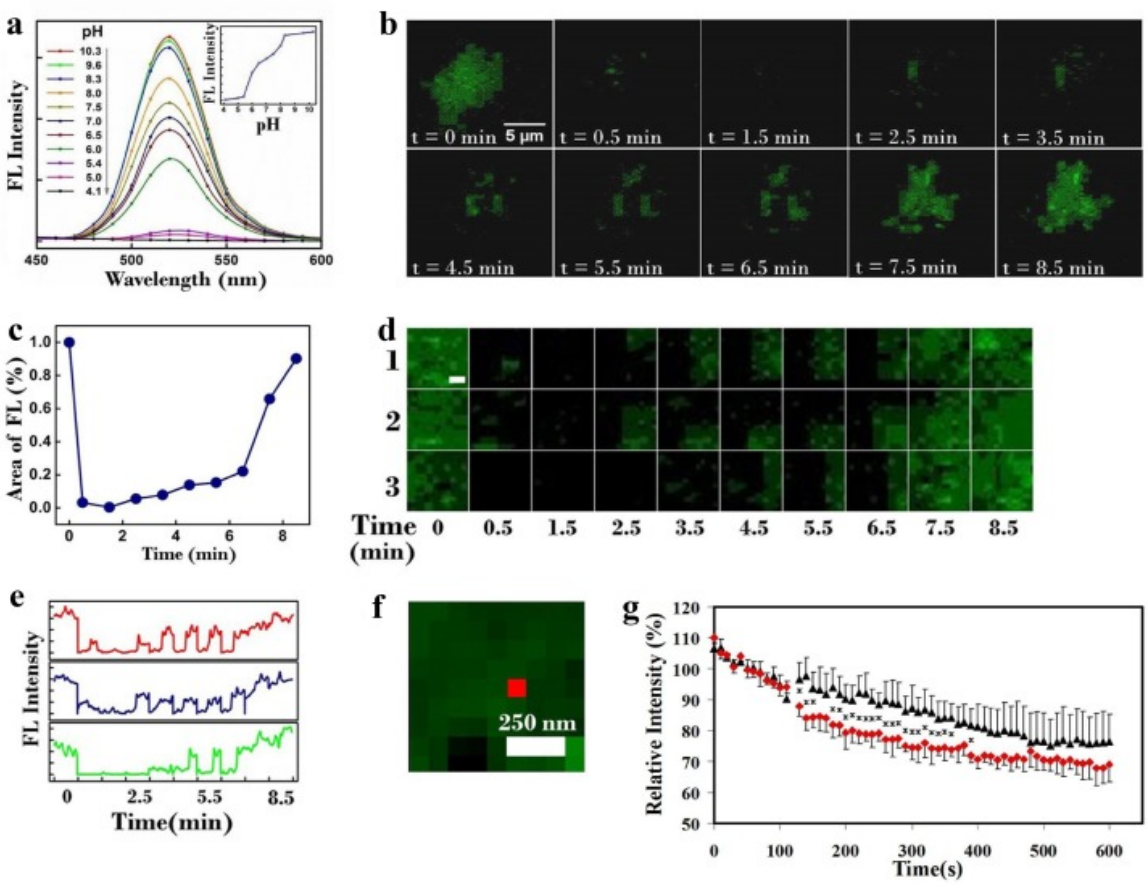

Figure 4.1: Glucose-stimulated insulin secretion of Min-6 cells induces an intracellular pH drop followed by alkalization, demonstrated using pH-sensitive CdTeQDs. (a) Green fluorescent cadmium telluride quantum dots (CdTeQDs) are pH sensitive. Note the near-linear increase in fluorescent intensity with increasing pH of the suspension medium (pH 5.5 to pH 9). (b) Exposure of insulin secreting MIN6 cells loaded with CdTeQDs to glucose, results in a time-dependent drop in fluorescence as a consequence of a decrease in intracellular pH, followed by alkalization and return of fluorescence within 8-10 min. (c, d) Fluorescent intensity of cells plotted following glucose exposure demonstrate a sharp drop in fluorescence (indicating a pH drop) within the first min, followed by a gradual rise in fluorescent intensity (alkalization) in 7 min, followed by a sharp rise and return to resting pH in 9-10 min. (d) Three randomly picked fluorescent areas in (b) at increased resolution, demonstrate an initial drop in pH followed by increase, after stimulation of insulin secretion and (e) fluorescent intensity line scans of the shown areas. (f) A single pixel size of 80 nm (red square) is obtained in the fluorescent images. (g) Spectrofluorimetry of suspended CdTeQD treated Min-6 confirms pH drop after glucose stimulation (red dots) but not with vehicle control (black dots) (*p<0.05).

To determine the relative intracellular pH changes *in vivo*, during glucose stimulated insulin secretion in MIN6 cells, cultured cells were preloaded with CdTeQDs and exposed to 35mM glucose stimulation. Fluorescent intensity, of images captured every minute from 0.5 to 8.5 minutes post stimulation, was measured. Intracellular fluorescence measurements demonstrated rapid initial acidification within the first minute after glucose stimulation, followed by a gradual recovery in intracellular pH in the subsequent 8 minute period to near resting levels (Figure. 4.1 b-e). Glucose induced intracellular acidification is demonstrated at high magnification with each pixel measuring 80 nm (Figure. 4.1 f). A similar trend was observed using spectrofluorimetry of suspended MIN6 cells preloaded with CdTeQDs where glucose addition induced a significant drop in intracellular pH followed by gradual recovery when compared to vehicle controls (Figure. 4.1 g).

To test the status of t-/v-SNARE complexes at various intervals following glucose stimulated insulin secretion from MIN6 cells, Western blot analysis on total cell homogenates were performed using a syntaxin specific antibody (Figure 4. 2 a).

Result from this study demonstrated greater amounts of complexed SNAREs in the early acidic phase (1 minute following stimulation of secretion), compared to the later alkaline phase (10 minute) following glucose stimulation (Figure 4.2 a). To further test the role of pH on the SNARE complex in a separate tissue, the direct role of pH in ATP mediated dissociation of native brain t-/v-SNARE-NSF complex, was assessed. To perform this test, t-/v-SNARE-NSF complexes were immunoisolated from rat brain tissue and subjected to ATP in either acidic (pH 6.0) or basic (pH 7.4) environment (Figure 4.2 b-d). Lower pH clearly demonstrated its inhibitory effect on ATP mediated dissociation of

NSF from the native t-/v-SNARE-NSF complex as observed in Western blot analysis using a NSF-specific antibody (Figure 4.2 c, d).

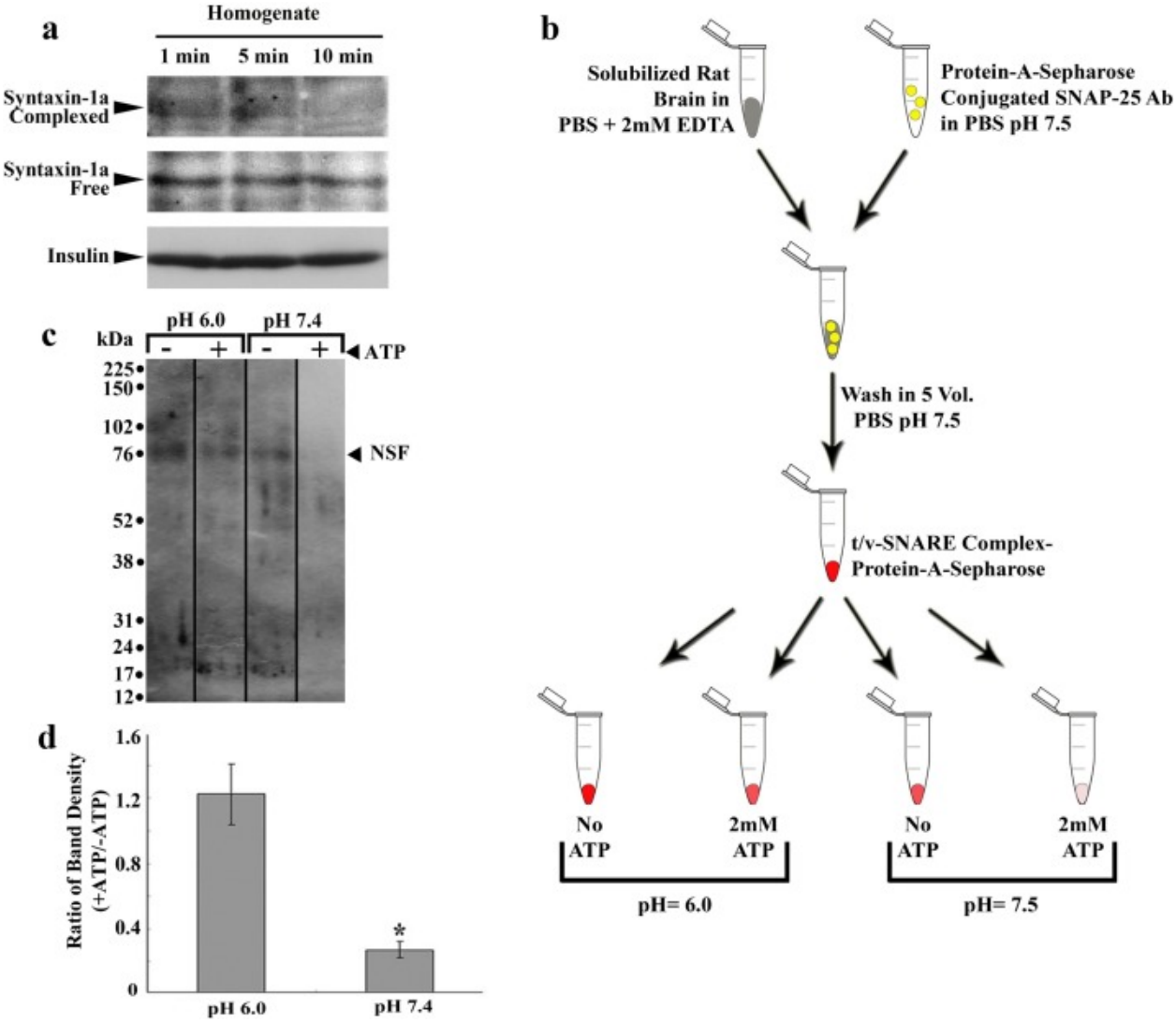

Figure 4.2: NSF-ATP mediated t-/v-SNARE complex disassembly is attenuated in acidic pH environment. (a) Immunoblot analysis of MIN6 cell lysate using Synataxin-1A antibody on homogenates of cells following 1 min, 5 min, and 10 min of glucose stimulation, demonstrate a loss in complexed syntaxin at the 10 min time point. Note equal protein loads of each homogenate fraction as demonstrated using insulin-specific antibody. (b) Schematic outline of the experiment to isolate SNARE-NSF complex from rat brain tissue, and their dissociation at pH 6.0 and 7.4 in presence of ATP. (c) Immunoblot analysis using NSF-specific antibody demonstrate inhibitory effect of low pH on ATP-induced dissociation of NSF from native rat brain t-/v-SNARE-NSF complex. NSF immunoblot analysis of t-/v-SNARE-NSF complex at pH 6 and 7.4 in presence and absence of ATP was resolved using SDS-PAGE and transfer to nitrocellulose membrane and probed using NSF-specific antibody. Note the complete dissociation of NSF from the complex at pH 7.4 in presence of ATP as opposed to pH 6.0. The data presented in 2c is from the same Western blot. (d) Bar graph of NSF immunoreactivity in t-/v-SNARE-NSF complex shows a significant loss at pH 7.4 (n=4) (*p<0.01).

Next the role of pH on the ability of NSF-ATP to dissociate the SNARE complex

was further tested using purified recombinant NSF and full-length recombinant t-SNAREs- and v-SNARE reconstituted into liposomes (Figure 4.3 a-c). SNARE reconstituted PC: PS liposome suspension in PBS either at pH 6.0 or 7.4 were exposed to NSF-ATP, and their interaction status was examined using AFM (Figure 4.3 a-c) and photon correlation spectroscopy (PCS) (Figure 4.3 d, e). Liposome size influences membrane curvature, and the interacting surface between opposing vesicle membrane are dictated by the size of the t-/v-SNARE rosette complex[73]. Hence, liposomes of uniform size were prepared using a published extrusion method, and used to reconstitute purified full-length recombinant t- and v-SNAREs for the study[32]. AFM examination of bare PC: PS liposomes (Figure 4.3 a), demonstrated vesicle size to range between 42 nm and 62 nm, with an average size of 52 nm. Two sets of PC: PS liposomes (50 nm diameter), one set reconstituted with t-SNAREs (syntaxin and SNAP-25) and the other reconstituted with v-SNAREs, were used. AFM imaging studies demonstrated that addition of ATP to NSF containing suspensions of t-SNARE and v-SNARE liposomes in PBS at pH 7.4 resulted in dissociation of a majority of the t-/v-SNARE complexes. Consequently, vesicles formed dimers as opposed to pentamers observed at pH 6.0 (Figure 4.3 b). The AFM results were further corroborated using PCS studies (Figure 4.3 d). In agreement, PCS results demonstrated that liposomes at both low and neutral pH assembled into clusters of 4-5 (228-231 nm) in absence of ATP. However, addition of ATP to the SNARE-reconstituted liposome suspension at pH 6.0 resulted in a near doubling of cluster size (352 nm), whereas at pH 7.4, a 50% reduction in cluster size (112 nm) was observed (Figure 4.3 d). The findings from AFM and PCS studies substantiate our results obtained using native neuronal SNARE complex. It further upholds our hypothesis that the initial establishment

of low intracellular pH upon stimulation of cell secretion, may serve as a block on NSF-ATP mediated t-/v-SNARE disassembly (Figure 4.3 f). This low pH environment established immediately following stimulation of cell secretion, results in docked vesicles stably engaged with the cell plasma membrane via the SNARE complex, enabling vesicle fusion and content release.

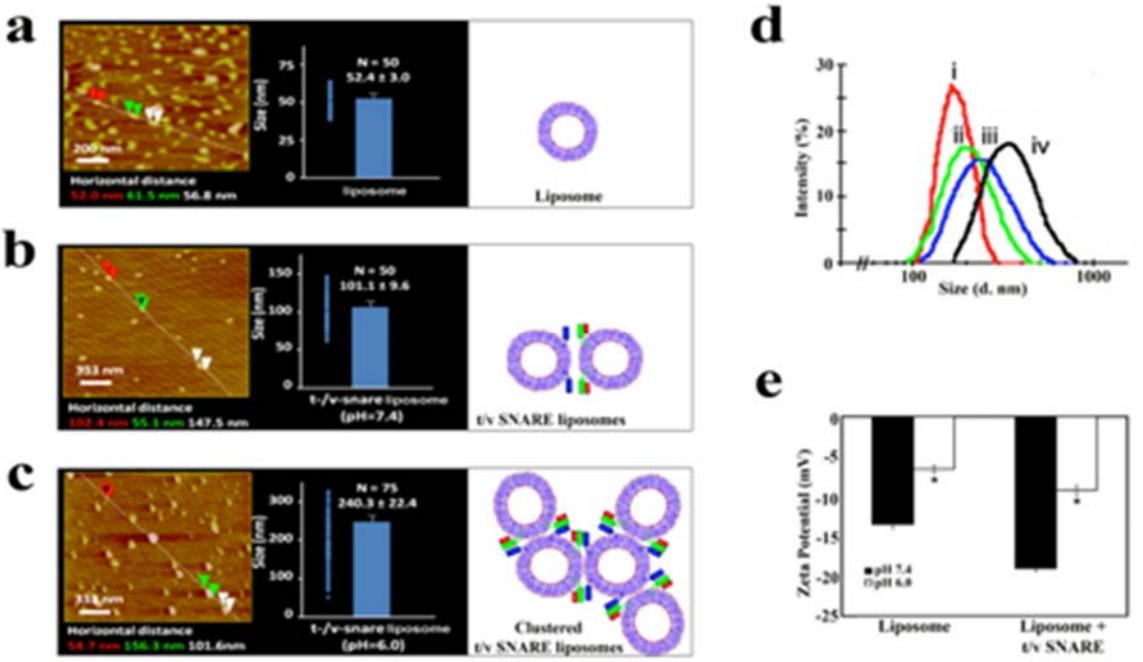

Figure 4.3. Association between t-SNARE liposomes and v-SNARE liposomes in presence of NSF-ATP is governed by pH. (a) Representative AFM micrographs of bare 50 nm PC:PS liposomes; (b) t-SNARE and v-SNARE reconstituted liposomes at pH 7.4, and (c) at pH 6.0 following exposure to NSF-ATP. The average size of PC:PS liposomes are 52 nm, with a distribution between 42 and 62 nm. Blue dots to the left represent size of each liposome clusters in nm. Note following exposure to NSF-ATP at pH 7.4, SNARE-reconstituted liposomes are present as dimers, as opposed to pentamers at pH 6.0. (d) PCS using Zeta sizer confirms AFM results. t-SNARE and v-SNARE reconstituted 50 nm PC:PS liposomes, demonstrating NSF-ATP mediated SNARE complex disassembly result in dissociation of liposome clusters at pH 7.4 (green, ii to red, i). The average Z size of the proteoliposome clusters at pH 7.4 measure 228 nm before NSF-ATP addition and 112 nm following NSF-ATP exposure (green, ii to red i), conforming AFM results in a. In contrast, the average Z size of liposome clusters at pH 6.0 measure 231 nm prior to NSF-ATP addition and 351 nm following exposure to NSF-ATP, as observed in the AFM studies. (blue, iv to black, iii). (e) Surface charge of 50 nm PC:PS liposomes drop following SNARE reconstitution, and nearly a 50% drop in negative surface charges are observed in both populations of liposomes (bare and SNARE-associated) at pH 6.0 compared to at pH 7.4 (n=8) (*$p<0.05$). (f) Schematic of t/v SNARE-reconstituted liposome clustering behavior in presence of NSF-ATP at pH 7.4 and pH 6.0.

Given the known capability of NSF to oligomerize in presence of ATP[77], one would speculate that the observed doubling of t-/v-SNARE-NSF vesicle clusters at pH 6.0

following ATP addition may reflect interactions between NSF-ATP molecules associated with the vesicle-SNARE complexes. Protein structure, and hence protein function, is greatly influenced by the pH of its surrounding environment. To test if pH induces any major changes to the net surface charge of vesicle-associated SNAREs, zeta potential measurements were performed (Figure. 4.3 e)[84]. SNARE-reconstituted liposomes had relatively more negative zeta potential value compared to bare 50 nm PC: PS liposomes at both pH 7.4 and 6.0. However, both liposome populations demonstrated a 50% drop in the net negative charge when transferred from pH 7.4 to pH 6.0 (Figure. 4.3 e). This 50% reduction in net charge, observed both in bare and SNARE-associated liposomes suggests that pH of the dispersion medium primarily contributes to the surface charge on liposomes rather than that of the vesicle-associated SNARE proteins.

Our results reveal a mechanism where changes in intracellular pH, reflected in the rapid intracellular acidification followed by gradual alkalization during cell secretion, governs the assembly and disassembly of the SNARE membrane fusion protein complexes. These results suggest that the loss in NSF-ATP induced SNARE disassembly at pH 6.0 is likely a consequence of a loss in the ATPase activity of NSF, abrogating the ability of NSF to disassemble the SNARE complex. Structural changes to the SNARE complex at low pH influencing NSF-ATP mediated disassembly is unlikely, given that the 50% reduction in net charge observed in both bare and SNARE-associated liposomes is found to be contributed by the pH of the dispersion medium on the surface charge of liposomes rather than on the vesicle-associated SNAREs. The status of the SNARE complex may be one of several proteins influenced by the pH drop that occur during cell secretion. For instance, the secretory vesicle-associated vH^+ ATPase is also found to be

critical for neurotransmitter release in neurons and insulin release from beta cells of the endocrine pancreas[32,85]. Moreover, intracellular acidification in yeast is known to stimulate vH^+ ATPase activity[86], supporting the hypothesis that an intracellular drop in pH following stimulation of cell secretion is also a requirement for vH^+ ATPase activation during cell secretion. Additional roles of intracellular pH dynamics following stimulation of cell secretion awaits discovery

CHAPTER 5: IDENTIFICATION OF AN EPILEPTIC DRUG THAT AFFECTS GLUCOSE STIMULATED INSULIN SECRETION

(This Chapter contains previously published material. See Appendix C)

Abstract

Valproate (VPA), an FDA approved anti-epileptic drug with a half-life of 12-18 hours in humans, has shown to perturb the vacuolar proton pump (vH^+ ATPase) function in yeasts by inhibiting myo-inositol phosphate synthase, the first and rate-limiting enzyme in inositol biosynthesis, thereby resulting in inositol depletion. vH^+ ATPase transfers protons (H^+ ions) across cell membranes, which helps maintain pH gradients within cells necessary for various cellular functions including secretion. This proton pump has a membrane (V0) and a soluble cytosolic (V1) domain, with the C-subunit associated with V1. In secretory cells such as neurons and insulin secreting beta cells, vH^+ ATPase acidifies vesicles essential for secretion. In this study, we demonstrated that exposure of insulin secreting MIN6 cells to a clinical dose of VPA results in inositol depletion and loss of co-localization of subunit C of vH^+ ATPase with insulin secreting granules. Consequently, a reduction of glucose-stimulated insulin secretion is observed following VPA exposure. These results merit caution and the reassessment of the clinical use of VPA.

Introduction

Valproate (VPA), an FDA approved drug with unknown mechanism of action, has been clinically used for the past four decades in treating migraines, bipolar disorders and epileptic seizures. Owing to its structural resemblance to gamma amino butyric acid (GABA), a master inhibitory neurotransmitter, VPA was initially thought to diminish neuro-excitability and regulate various neuronal pathways[87-89]. Known effects of VPA include

histone deacetylase (HDAC) inhibition, which alters neuronal gene expression[90,91]. Inositol depletion has recently been demonstrated in cells treated with VPA, similar to the action of lithium, a mood-stabilizing predecessor of VPA[92,93]. Inositol depletion is attributed to inhibition of myo-inositol phosphate synthase (MIPS), the rate-limiting enzyme in the inositol biosynthesis pathway[94,95]. Inositol is a precursor to secondary signaling messengers including inositol 1,4,5-trisphosphate (IP3) and diacylglycerol (DAG)[96-98]. A major consequence of VPA-induced inositol loss is its inhibitory effects on vH^+ ATPase as demonstrated in *Saccharomyces cerevisae*[36].

vH^+ ATPase is a large multi-subunit complex consisting of a membrane (V0) and cytosolic domain (V1), 260 kDa and 650 kDa respectively. V0, the proton translocator, consists of six subunits whereas V1, which hydrolyses ATP, consists of eight subunits[99]. vH^+ ATPase is present on the insulin secretory granule (ISG) membrane and functions similarly to its suggested role in neuronal synaptic vesicles[100]. It also capacitates ISGs, making them competent to secrete insulin, and similar to synaptic vesicles, ISG acidification is required for its maturation[101,102]. The vH^+ ATPase functions specifically to pump H^+ into ISGs with a simultaneous influx of Cl^- ions by ClC-3 channel, leading to an ATP-dependent priming of ISGs, facilitating insulin secretion[101]. Moreover, granule acidification is necessary for enzymatic function of PC1/3 and PC2 (pro-protein convertases) residing within ISGs, which produce mature insulin from its pro-hormone peptide[102]. Studies suggest vH^+ ATPase to be important for membrane fusion events involving SNARE proteins[103,104]. Therefore, prevention of ISG acidification interrupts ISG maturation and its capability to fuse at the cell plasma membrane, leading to inhibited insulin release. Hence, we hypothesized that loss of vH^+ ATPase function in pancreatic β

cells, specifically in ISGs due to VPA induced inositol depletion, would lead to decreased glucose stimulated insulin secretion. In the current study, using mouse insulinoma (MIN6) cells, we demonstrated that VPA exposure indeed causes intracellular inositol depletion. This resulted in the inability of vH^+ ATPase cytosolic subunit C to assemble at the ISG membrane, precluding vH^+ ATPase activity, and the consequent loss of glucose-stimulated insulin secretion.

Experimental Procedures

Glucose Stimulated Insulin Secretion from MIN6 Cells in Culture

MIN6 cells were grown to confluence using sterile 100 x 13 mm plastic Petri dishes according to published procedure[60]. Cells were cultured in 25 mM glucose Dulbecco's Modified Eagle Medium (Invitrogen) containing 10% fetal calf serum, penicillin, streptomycin, and 50 μM β-mercaptoethanol. Cells were stimulated using 35mM glucose, and insulin secreted into the medium was collected at 10 and 30 min. Stimulation assays were performed following 0.5h, 2h, 5h, 16h, and 24h of exposure to 1mM VPA. All secretion assays were carried out at room temperature (RT), and cells were washed phosphate buffered saline (PBS) pH 7.4 prior to stimulation. Following glucose stimulation, 200uL aliquots of the PBS incubation medium were collected at 10 and 30 minutes post stimulation. Aliquots were centrifuged at 4,000 xg to remove any aspirated cells, and 160 μl of the supernatant was mixed with 40 μl of 5x Laemmli reducing sample preparation buffer[41] for Western blot assay. To obtain the total amount of insulin in cells, Min6 cells were solubilized in 100 μL of homogenization buffer (2mM EDTA, 2mM ATP, 0.02% Triton X-100, 1:500 protease inhibitor cocktail, pH 7.4) following secretion assays, and protein concentrations[61] were determined prior to Western blot analysis.

Estimation of Inositol in MIN6 Cells

Intracellular inositol levels were determined as described previously with modification[105]. Briefly, confluent MIN6 cell plates (3 per time point) were incubated with 1 mM VPA for 30 minutes, 2 hours, 5 hours, 16 hours, and 24 hours respectively. After incubation, cells were washed twice with ice-cold PBS and lysed in ice-cold water containing protease inhibitor. Cells were centrifuged at 16,000 xg for 10 minutes to remove cellular debris, and protein concentrations of the supernatants were determined[61]. Supernatant protein (400 µg) was mixed with 7.5% perchloric acid and stored on ice for 20 minutes. This mix was centrifuged at 10,000 x g for 10 minutes at 4 oC to remove protein precipitates. Supernatants containing cytosol were used for inositol measurement. Samples were centrifuged and loaded onto columns with 1 mL of AG 1-X8 resin/H2O (1:1) mixture. Inositol was eluted with 5 mL of H_2O. Eluates were dried in an oven at 70 ^oC, stored at -80 ^oC. Prior to assay, samples were dissolved in dH_2O and inositol levels were measured using the Maslanski and Busa Method[106].

Immunocytochemistry

MIN6 cells were grown on 35 mm glass bottom Petri dishes for immunocytochemistry[60]. The distribution of vH^+ ATPase -C1 subunit and ISGs in 1 mM VPA-treated (5 hours at 37 ^oC) MIN6 cells were compared with vehicle-treated control (PBS) MIN6 cells. Primary antibodies, rabbit polyclonal anti vH^+ ATPase -C1 (SC 20944) and mouse monoclonal anti-insulin (SC 8033), and secondary antibodies, donkey anti-rabbit AF 594 and donkey anti-mouse AF 488 (Life Technologies), were used in the study. Cells were exposed to DAPI nuclear stain for nucleus localization. An immunofluorescence FSX100 Olympus microscope was used to acquire immuno-

fluorescent images through a 63x objective lens (numerical aperture, 1.40) with illumination at 405, 488, or 647nm. Insulin and vH-ATPase localization and cellular distribution were obtained through merging fluorescent images using Imagej.

Results and Discussion

VPA first came into medical use in 1962 and although its molecular mechanism of action is far from fully understood, it is listed in the World Health Organization as a safe and essential medicine[107]. Recent advances in understanding its mechanism of action have revealed perturbation of yeast vH^+ ATPase function as a consequence of VPA-induced inositol depletion[94]. The current study confirms this finding in a mammalian cell, demonstrating that clinical levels of VPA exposure decreases inositol levels in MIN6 cells. VPA-treated MIN6 cells from various incubation time points (Figure 5.1A) demonstrated a significant decline in inositol after 5h (Figure 5.1B). VPA has previously[108] been shown to deplete inositol by inhibiting MIPS, the first and rate-limiting enzyme of inositol biosynthesis.

In agreement with VPA-induced inositol depletion, disrupts vacuolar morphology and hence function in wild-type yeast cells[36], valproate reduces vH^+ ATPase subunit C1 localization to ISG. vH^+ ATPase is localized to the ISG membrane in β cells of pancreatic islets[85,100,102]. Similar to neuronal synaptice vesicles, granule acidification is important for insulin release. Glucose stimulation lowers intraluminal ISG pH, and pharmacological inhibitors of vH^+ ATPase block this effect[85,101,102,109]. Further, studies have demonstrated reduced plasma insulin levels in *oc/oc* mice. The *oc/oc* mice carry a mutation for a3 isoform of V0 domain[85]. The assembly of the various vH^+ ATPase subunits is a highly orchestrated process and depends on the cell's functional requirements[110].

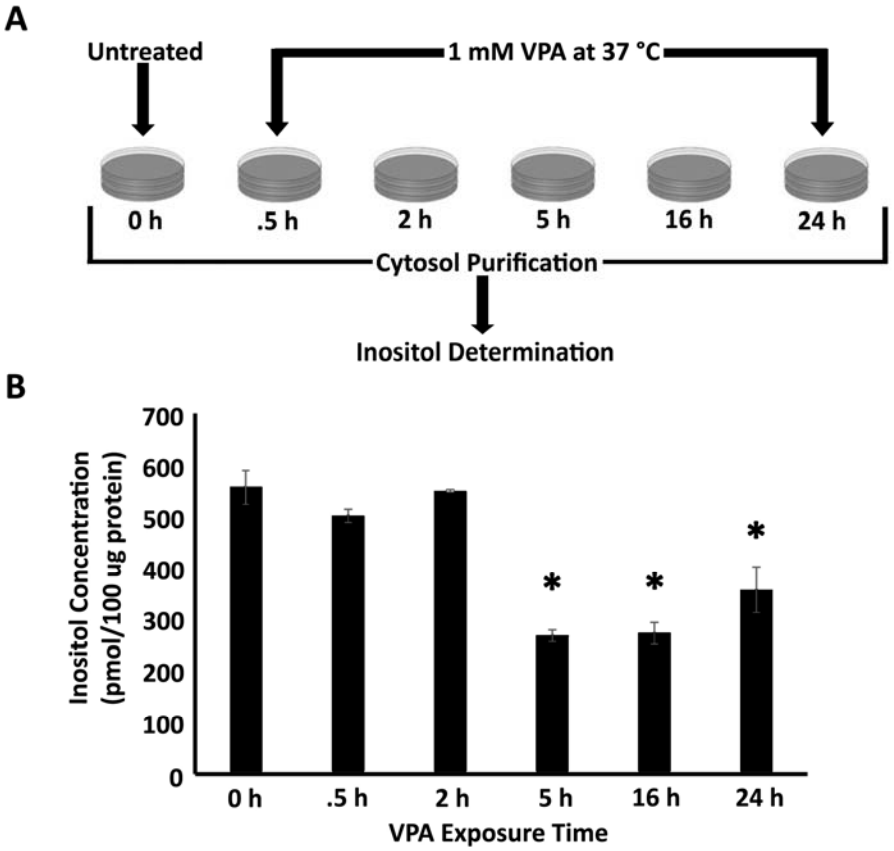

Figure 5.1: Inositol depletion in MIN6 cells is observed following 5 hours of VPA exposure. A: Schematic diagram showing MIN6 cells growing in culture dishes for different periods of VPA exposure. Inositol is determined in the extracted cell cytosol. **B:** Inositol concentrations in MIN6 cell cytosol show significantly decreased intracellular inositol levels first after 5h of 1mM VPA treatment (n=3, $p < 0.05$).

For example, V1 association with V0 is glucose dependent in yeast as well as in porcine (HK-2) and mammalian kidney cells (LLC-PK1), while phosphoinositide 3-kinase (PI3K) inhibition is known to impede this outcome[37]. Therefore, in the current study, we wanted to determine the consequences of VPA induced inositol depletion on MIN6 vH^+ ATPase organization. Since at the 5-hour time point following VPA exposure shows a significant drop in inositol in the cell cytosol (Figure 5.1), the distribution of insulin-containing granules and the subunit C of vH^+ ATPase was examined in MIN6 cells. Immunofluorescence labeling of MIN6 cells (Figure 5.2 A-E) demonstrated co-localization of the vH^+ ATPase subunit C^2 with insulin (green) containing ISGs. In contrast, double immunofluorescence labeling of VPA-treated MIN6 cells (Figure 5.2 F-J) demonstrated substantially diminished co-localization of the vH^+ ATPase subunit C^2 with insulin (green)

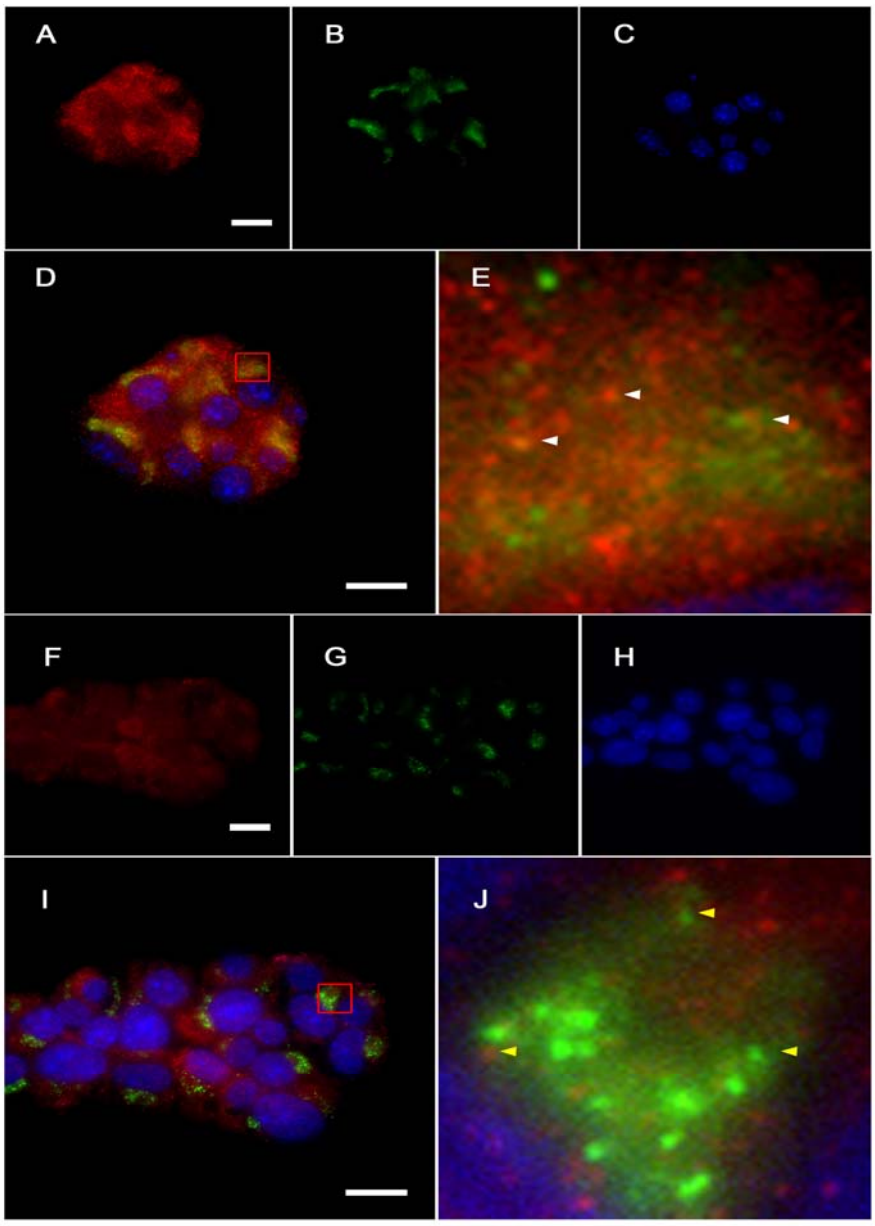

Figure 5.2: Decreased co-localization of vH$^+$-ATPase subunit C with insulin in VPA-treated MIN6 cells. A-C: Immunofluorescent images of control MIN6 cells labeled with the nuclear stain DAPI (blue) and antibodies against vH$^+$ ATPase C subunit (red) and insulin (green). **D**: Composite image of MIN6 cells labeled with DAPI, vH$^+$ ATPase, and insulin. Note the co-localization of insulin in insulin granule and the C subunit of the vH$^+$ ATPase. **E**: Digitally zoomed inset from D; white arrows indicate increased vH$^+$ ATPase subunit C and insulin co-localization. **F-H**: Immunofluorescent images of 5h 1mM VPA-treated MIN6 cells labeled with DAPI and antibodies against vH$^+$-ATPase C-subunit and insulin. **I**: Composite image of MIN6 cell labeled with DAPI, vH$^+$ ATPase, and insulin. **J**: Digitally zoomed inset from I; yellow arrows indicate individual vH$^+$ ATPase and insulin puncta. Note there is little co-localization of vH$^+$ ATPase and insulin. *Scale bar = 15 µm*.

containing ISGs. Additionally, ISGs appear to localize to the center of the cell following VPA treatment and fail to traffic to the plasma membrane unlike normal competent ISGs

observed in control cells. These results are noteworthy because subunit C, together with the other cytosolic subunits, needs to be assembled in the cellular membrane for a fully functional vH^+ ATPase. Relative absence of subunit C from ISG membrane of VPA-induced inositol-depleted cells compromises vH^+ ATPase assembly and activity, would negatively impact cell secretion.

Several studies attest to the knowledge that vH^+ ATPase provides the electrochemical proton gradient for neurotransmitter uptake, storage, and ultimately release by a synaptic vesicle[111-115].

Therefore, we wanted to study the influence of VPA on insulin secretion from β cells. Glucose-stimulated insulin secretion from MIN6 cells measured at various time points post-VPA treatment demonstrated loss in insulin release compared to untreated control cells (Figure 5.3). Additionally, a significantly lower rate of insulin release was

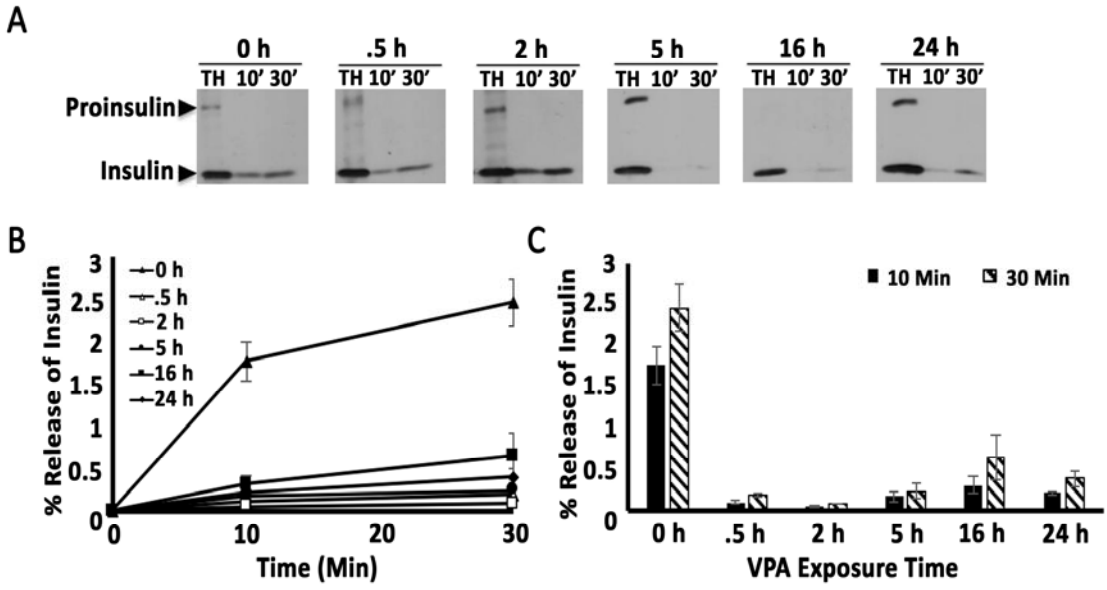

Figure 5.3: VPA treatment significantly reduces glucose-stimulated insulin secretion in MIN6 cells. **A**: Representative western blots of MIN6 cell total homogenate (TH) and insulin secretions collected at 10 and 30 minutes after glucose stimulation in control and 1mM VPA-treated cells. **B-C:** Note the significant decrease in percent release of total cellular insulin at 10 and 30 minutes post-glucose stimulation following 30min, 2h, 5h, 16h, and 24h of exposure to VPA (n=3, $p< 0.05$).

observed in VPA-treated cells compared to controls (Figure 5.3 B). The percent release

of total cell insulin was substantially lower at both 10 min and 30 min following glucose stimulation of VPA-treated cells compared to controls (0h) (Figure 5.3 A-C). In summary, these studies demonstrate the detrimental effect of VPA on cell secretion. VPA exposure

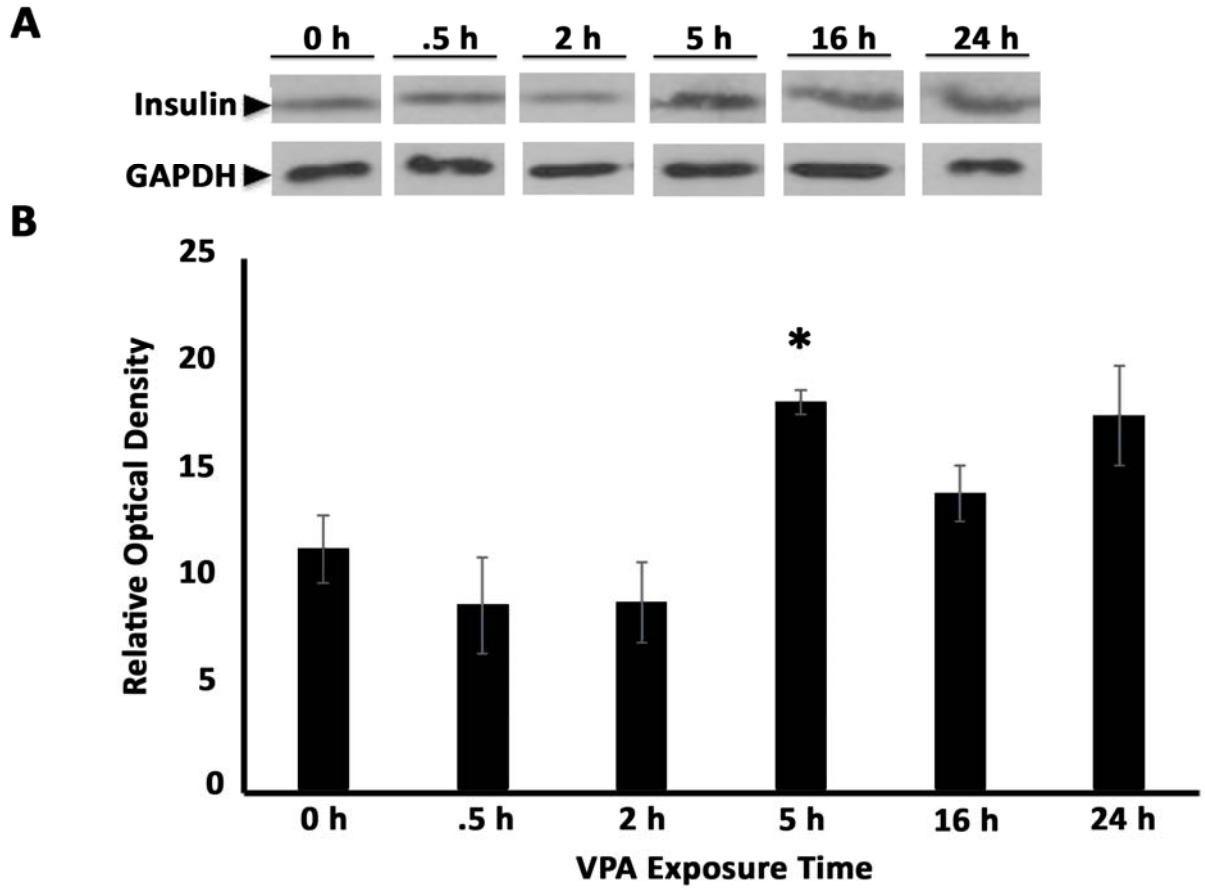

Figure 5.4: VPA treatment increases total intracellular insulin content in MIN6 cells. A: Representative Western blots of MIN6 cell homogenate from control and VPA-treated MIN6 cells at various time points. **B:** Total intracellular insulin significantly increases after 5h of VPA treatment, suggesting the cellular accumulation of insulin due to a loss in the ability of the cell to secrete (n=3, $p < 0.05$).

significantly lowered glucose-stimulated insulin release from MIN6 cells as observed using Western blot analysis. Conventionally, ELISA assays are performed to estimate insulin, however in the current study Western blots were used to estimate insulin release since ELISA assays will be unable to differentiate insulin from non-secretory proinsulin that may be released into the medium as a possible consequence of cell lysis. Our study

further demonstrated that VPA treatment resulted in the accumulation of insulin in MIN6 cells. We analyzed total cellular insulin content in MIN6 cells post 1mM VPA treatment to understand whether loss in secretion was due to fusion incompetence of the ISGs or reduced insulin biosynthesis. Western blot analysis shows a significant increase in insulin content in total MIN6 cell lysate after 5 h of 1 mM VPA treatment compared to untreated control cells (Figure 5.4 A, B). Immuno-GAPDH signal is used as a loading control, demonstrating equal loading of cell lysate. Hence, insulin synthesis in VPA-treated cells appears to be normal; however, ISGs are unable to optimally secrete their intra-granular contents, leading to loss of insulin secretion and their consequent accumulation in cells.

To our knowledge, this is the first demonstration of inositol depletion and the loss of insulin function in pancreatic β cells treated with a clinical dosage of VPA. A fully assembled vH^+ ATPase leading to ISG granule acidification is required for insulin secretion[114]. Dissociation of the soluble C subunit from the vH^+ ATPase complex at the ISG in valproate-treated MIN6 cells observed using immunocytochemistry, further supports the requirement of a fully assembled vH^+ ATPase at the ISG in insulin secretion from β cells. We chose to examine subunit C of the proton pump as an indicator of assembly/disassembly, since it is a soluble subunit present in the peripheral stalk of the eukaryotic proton pump. Furthermore, when vH^+ ATPase disassembles, it is known to separate into a V0 domain, V1 domain (without subunit C), and subunit C of V1 domain[99,116]. Thus, incorporation of subunit C is the final step in assembly of a fully assembled and functional vH^+ ATPase pump.

Our demonstration of a loss in insulin secretion from MIN6 cells upon VPA exposure suggests that the VPA effect is not due to a decrease in insulin synthesis, since

an increase in total cellular insulin was observed in these cells as a consequence of a loss in its ability to secrete. Close examination of immunostained cells shows that majority of insulin is localized centrally and at the perinuclear region, suggesting their presence in the Golgi, and their inability to be appropriately packaged into secretory vesicles in VPA-treated cells. Additionally, it could mean that the granules are somehow incompetent to traffic away from the Golgi toward the plasma membrane for fusion and secretion. Further studies using mouse and human islets are in progress to confirm these observations, including the use of expansion microscopy for obtaining nanometer scale distribution of various components of the vH^+ ATPase pump. In summary, we demonstrate that clinical dose of VPA leads to a loss in glucose-stimulated insulin secretion from MIN6 cells. This loss is due in part to the incomplete assembly of vH^+ ATPase at the ISG membrane as a consequence of VPA treatment. It is likely that inhibition of vH^+ ATPase by VPA was due to inositol depletion, as shown in yeast. Since vH^+ ATPase provides the electrochemical proton gradient for neurotransmitter uptake, storage, and ultimately release by a synaptic vesicle, we speculate that VPA action may occur by reducing neurotransmitter release by altering vH^+ ATPase activity as a consequence of inositol depletion, thereby abrogating seizures in epileptic patients[111-115]. It is to be noted, that since VPA has a half-life of nearly 16h and in some cases administered daily to both adults and children, sometime for a period of two weeks, its detrimental effects observed at very early time points in our study is alarming. Results from the current findings therefore however merit caution and the careful reassessment of the clinical use of VPA.

CHAPTER 6: DISCUSSION AND CONCLUSIONS

For decades, the prevailing worldview was that secretion operates as an all-or-none ‘total fusion’ event, where secretory vesicles are trafficked to the cell surface where the membrane encapsulating the secretory vesicle fuse and completely incorporate into the cell plasma membrane. The vesicle contents then diffuse out of the cell. This hypothesis, although attractive at first glance, had several key setbacks. (i) First, it predicted a quantization of secretory products packaged into each secretory vesicle, when in fact, secretory vesicle size greatly vary even within the same cell, sometimes as much as 6-fold. (ii) Second, the level of additional regulation necessary to rapidly and precisely internalize and sequester vesicle-associated lipids and proteins following incorporation into the cell plasma membrane seem extraordinarily complex, given the tens of thousands of different membrane lipids and their differential distribution even between the same bilayer leaflets. (iii) Third, following a secretory episode, partially empty secretory vesicles accumulate within cells as observed in electron micrographs, demonstrating that secretory vesicles are capable of partial content release.

Therefore, the discovery of porosome was paramount, in our understanding of the transient or the kiss-and-run cell secretory mechanism. Porosome is a supramolecular universal secretory portal, which we also demonstrated in insulin secreting MIN6 cells. Importantly, for the first time, we were able to reconstitute immunoisolated MIN6 porosomes into live MIN6 cells. We demonstrated that the MIN6 porosomes are stably reconstituted and are able to potentiate glucose stimulated insulin secretion of MIN6 cells.

We demonstrated that following glucose stimulation, a drop in intracellular pH is observed. While this drop in pH may play multiple roles, our goal was to understand its

importance in SNARE complex assembly/ disassembly. We demonstrated that the relatively lower pH inactivates an enzyme known as ‘NSF’, which is an ATP utilizing enzyme causing disassembly of the t/v SNARE protein complex. NSF was immuno-isolated with other SNARE complex proteins at an acidic pH of 6.0, while it did not immune-isolate at a relatively basic pH of 7.4. Thus, the lower pH propagates cell secretion by locking the NSF with the SNARE protein complex initially and finally releasing it once its function is achieved. Following secretion, the cellular pH returns to relatively basic levels, activating NSF, disassembling the SNAREs, thus terminating cell secretion. Further, the drop in pH might not occur uniformly throughout the cell, but rather in certain regions of the cell forming a gradient of various pHs, however the impact of such pH gradient this remains to be investigated.

The regulation of pH occurs not just within cells but also within the secretory vesicles. A bafilomycin sensitive drop in pH was observed within the insulin secreting granules. When intragranular pH drop was arrested using bafilomycin A, glucose stimulated insulin release was reduced.

These results led to the final aim of investigating valproate, an anti convulsing agent used for treatment of several neurological disorders. It was previously reported that valproate disrupts the function of the proton pump v-H^+ ATPase in yeasts by inhibiting the enzyme myoinositol phosphate synthase (MIPS), involved in the rate limiting step of inositol biosynthesis. Since v-H^+ ATPase is present at the insulin secreting granule membrane, we hypothesized and further demonstrated disruption of insulin secretion upon treatment with this drug. Additionally, we also demonstrated that valproate causes

one of the cytosolic subunits of the pump to de-localize with the ISGs as compared to normal untreated cells thereby inhibiting insulin secretion.

Although this study provides an impressive account of the importance of pH in regulation of insulin secretion, there still is a major gap of knowledge in the steps leading to pH regulation. We demonstrated the role of vH^+ ATPase in lowering ISG pH but the upstream signaling mechanisms that activate vH^+ ATPase in insulin secreting cells is yet unknown. In synaptic vesicles it has been established that vH^+ ATPase is under the control of a heterotrimeric G protein[81]. We know that Gi and Go are localized on ISG membrane but the heterotrimeric G protein that activates the proton pump during stimulation of secretion is not known. Conventionally, heterotrimeric G proteins are associated with a transmembrane receptor. If vH^+ ATPase is under the control of G protein in an insulin-secreting cell, the receptor that activates it is yet to be identified. Additionally, vH^+ ATPase in turn activates aquaporins, which fills water molecules into synaptic vesicles thus increasing their volume. Whether ISGs have a similar mechanism and if they do, it will be important to know the aquaporin isoform that implements this regulation. Thus, regulation at every step of the late secretory pathway is critical to glucose stimulated insulin secretion.

APPENDIX A

Copyright License Agreement for Chapter 2

OXFORD UNIVERSITY PRESS LICENSE
TERMS AND CONDITIONS

Jul 22, 2019

This Agreement between Wayne State University -- AKSHATA NAIK ("You") and Oxford University Press ("Oxford University Press") consists of your license details and the terms and conditions provided by Oxford University Press and Copyright Clearance Center.

License Number	4634350932227
License date	Jul 22, 2019
Licensed content publisher	Oxford University Press
Licensed content publication	Endocrinology
Licensed content title	Functional Reconstitution of the Insulin-Secreting Porosome Complex in Live Cells
Licensed content author	Naik, Akshata R.; Kulkarni, Sanjana P.
Licensed content date	Jan 1, 2016
Type of Use	Thesis/Dissertation
Institution name	
Title of your work	Molecular machinery for the 'kiss and run' mechanism of insulin secretion
Publisher of your work	Wayne State University
Expected publication date	Jul 2019
Permissions cost	0.00 USD
Value added tax	0.00 USD
Total	0.00 USD
Title	Molecular machinery for the 'kiss and run' mechanism of insulin secretion
Institution name	Wayne State University
Expected presentation date	Jul 2019
Portions	Entire text with all figures.
Requestor Location	Wayne State University 540 E Canfield St Room 5108 DETROIT, MI 48201 United States Attn: Wayne State University
Publisher Tax ID	GB125506730
Total	0.00 USD
Terms and Conditions	

STANDARD TERMS AND CONDITIONS FOR REPRODUCTION OF MATERIAL

APPENDIX B

Copyright License Agreement for Chapter 4

APPENDIX C

Copyright License Agreement for Chapter 5

SPRINGER NATURE LICENSE TERMS AND CONDITIONS

Jul 22, 2019

This Agreement between Wayne State University -- AKSHATA NAIK ("You") and Springer Nature ("Springer Nature") consists of your license details and the terms and conditions provided by Springer Nature and Copyright Clearance Center.

License Number	4634351217359
License date	Jul 22, 2019
Licensed Content Publisher	Springer Nature
Licensed Content Publication	Histochemistry and Cell Biology
Licensed Content Title	Valproate inhibits glucose-stimulated insulin secretion in beta cells
Licensed Content Author	Nikhil R. Yedulla, Akshata R. Naik, Keith M. Kokotovich et al
Licensed Content Date	Jan 1, 2018
Licensed Content Volume	150
Licensed Content Issue	4
Type of Use	Thesis/Dissertation
Requestor type	academic/university or research institute
Format	print and electronic
Portion	full article/chapter
Will you be translating?	no
Circulation/distribution	<501
Author of this Springer Nature content	yes
Title	Molecular machinery for the 'kiss and run' mechanism of insulin secretion
Institution name	Wayne State University
Expected presentation date	Jul 2019
Requestor Location	Wayne State University 540 E Canfield St Room 5108 DETROIT, MI 48201 United States Attn: Wayne State University
Total	0.00 USD
Terms and Conditions	

Springer Nature Customer Service Centre GmbH

REFERENCES

1 Delic, M. *et al.* The secretory pathway: exploring yeast diversity. *FEMS microbiology reviews* **37**, 872-914, doi:10.1111/1574-6976.12020 (2013).

2 Costa, T. R. D. *et al.* Secretion systems in Gram-negative bacteria: structural and mechanistic insights. *Nature Reviews Microbiology* **13**, 343, doi:10.1038/nrmicro3456 (2015).

3 Fesce, R., Grohovaz, F., Valtorta, F. & Meldolesi, J. Neurotransmitter release: fusion or 'kiss-and-run'? *Trends in cell biology* **4**, 1-4 (1994).

4 Jena, B. P. 'Porosome' discovered nearly 20 years ago provides molecular insights into the kiss-and-run mechanism of cell secretion. *Journal of cellular and molecular medicine* **19**, 1427-1440, doi:10.1111/jcmm.12598 (2015).

5 Ceccarelli, B., Hurlbut, W. P. & Mauro, A. Turnover of transmitter and synaptic vesicles at the frog neuromuscular junction. *The Journal of cell biology* **57**, 499-524 (1973).

6 Almers, W. & Tse, F. W. Transmitter release from synapses: does a preassembled fusion pore initiate exocytosis? *Neuron* **4**, 813-818 (1990).

7 Monck, J. R. & Fernandez, J. M. The exocytotic fusion pore. *The Journal of cell biology* **119**, 1395-1404 (1992).

8 Schneider, S. W., Sritharan, K. C., Geibel, J. P., Oberleithner, H. & Jena, B. P. Surface dynamics in living acinar cells imaged by atomic force microscopy: identification of plasma membrane structures involved in exocytosis. *Proceedings of the National Academy of Sciences of the United States of America* **94**, 316-321 (1997).

9 Jena, B. P., Cho, S. J., Jeremic, A., Stromer, M. H. & Abu-Hamdah, R. Structure and composition of the fusion pore. *Biophysical journal* **84**, 1337-1343, doi:10.1016/s0006-3495(03)74949-2 (2003).

10 Jeremic, A., Kelly, M., Cho, S. J., Stromer, M. H. & Jena, B. P. Reconstituted fusion pore. *Biophysical journal* **85**, 2035-2043, doi:10.1016/s0006-3495(03)74631-1 (2003).

11 Cho, W. J., Jeremic, A., Jin, H., Ren, G. & Jena, B. P. Neuronal fusion pore assembly requires membrane cholesterol. *Cell biology international* **31**, 1301-1308, doi:10.1016/j.cellbi.2007.06.011 (2007).

12 Cho, W. J. *et al.* Structure, isolation, composition and reconstitution of the neuronal fusion pore. *Cell biology international* **28**, 699-708, doi:10.1016/j.cellbi.2004.07.004 (2004).

13 Cho, W. J., Ren, G. & Jena, B. P. EM 3D contour maps provide protein assembly at the nanoscale within the neuronal porosome complex. *Journal of microscopy* **232**, 106-111, doi:10.1111/j.1365-2818.2008.02088.x (2008).

14 Cho, W. J., Lee, J. S. & Jena, B. P. Conformation states of the neuronal porosome complex. *Cell biology international* **34**, 1129-1132, doi:10.1042/cbi20100510 (2010).

15 Lee, J. S., Cho, W. J., Jeftinija, K., Jeftinija, S. & Jena, B. P. Porosome in astrocytes. *Journal of cellular and molecular medicine* **13**, 365-372, doi:10.1111/j.1582-4934.2008.00334.x (2009).

16 Cho, S. J. *et al.* Structure and dynamics of the fusion pores in live GH-secreting cells revealed using atomic force microscopy. *Endocrinology* **143**, 1144-1148, doi:10.1210/endo.143.3.8773 (2002).

17 Hou, X. *et al.* Proteome of the porosome complex in human airway epithelia: interaction with the cystic fibrosis transmembrane conductance regulator (CFTR). *Journal of proteomics* **96**, 82-91, doi:10.1016/j.jprot.2013.10.041 (2014).

18 Rajagopal, A. *et al.* Proteome of the insulin-secreting Min6 cell porosome complex: Involvement of Hsp90 in its assembly and function. *Journal of proteomics* **114**, 83-92, doi:https://doi.org/10.1016/j.jprot.2014.11.010 (2015).

19 Lewis, K. T., Maddipati, K. R., Naik, A. R. & Jena, B. P. Unique Lipid Chemistry of Synaptic Vesicle and Synaptosome Membrane Revealed Using Mass Spectrometry. *ACS chemical neuroscience* **8**, 1163-1169, doi:10.1021/acschemneuro.7b00030 (2017).

20 Fava, E. *et al.* Novel standards in the measurement of rat insulin granules combining electron microscopy, high-content image analysis and in silico modelling. *Diabetologia* **55**, 1013-1023, doi:10.1007/s00125-011-2438-4 (2012).

21 Nadelhaft, I. Measurement of the size distribution of zymogen granules from rat pancreas. *Biophysical journal* **13**, 1014-1029, doi:10.1016/S0006-3495(73)86042-4 (1973).

22 Kabachinski, G. & Schwartz, T. U. The nuclear pore complex--structure and function at a glance. *Journal of cell science* **128**, 423-429, doi:10.1242/jcs.083246 (2015).

23 Toft-Bertelsen, T. L., Ziomkiewicz, I., Houy, S., Pinheiro, P. S. & Sorensen, J. B. Regulation of Ca2+ channels by SNAP-25 via recruitment of syntaxin-1 from plasma membrane clusters. *Molecular biology of the cell* **27**, 3329-3341, doi:10.1091/mbc.E16-03-0184 (2016).

24 Han, J., Pluhackova, K. & Bockmann, R. A. The Multifaceted Role of SNARE Proteins in Membrane Fusion. *Frontiers in physiology* **8**, 5, doi:10.3389/fphys.2017.00005 (2017).

25 Jena, B. P. in *Methods in Cell Biology* Vol. 90 183-198 (Academic Press, 2008).

26 Schmauder-Chock, E. A. & Chock, S. P. Mechanism of secretory granule exocytosis: can granule enlargement precede pore formation? *The Histochemical journal* **19**, 413-418 (1987).

27 Zimmerberg, J. & Whitaker, M. Irreversible swelling of secretory granules during exocytosis caused by calcium. *Nature* **315**, 581-584, doi:10.1038/315581a0 (1985).

28 Whitaker, M. & Zimmerberg, J. Inhibition of secretory granule discharge during exocytosis in sea urchin eggs by polymer solutions. *The Journal of physiology* **389**, 527-539 (1987).

29 Jena, B. P. *et al.* G_i regulation of secretory vesicle swelling examined by atomic force microscopy. *Proceedings of the National Academy of Sciences* **94**, 13317, doi:10.1073/pnas.94.24.13317 (1997).

30 Arnaoutova, I. *et al.* Aquaporin 1 is important for maintaining secretory granule biogenesis in endocrine cells. *Molecular endocrinology (Baltimore, Md.)* **22**, 1924-1934, doi:10.1210/me.2007-0434 (2008).

31 Cho, S. J. *et al.* Aquaporin 1 regulates GTP-induced rapid gating of water in secretory vesicles. *Proceedings of the National Academy of Sciences of the United States of America* **99**, 4720-4724, doi:10.1073/pnas.072083499 (2002).

32 Shin, L. *et al.* Involvement of vH(+)-ATPase in synaptic vesicle swelling. *Journal of neuroscience research* **88**, 95-101, doi:10.1002/jnr.22180 (2010).

33 Pejler, G., Hu Frisk, J. M., Sjostrom, D., Paivandy, A. & Ohrvik, H. Acidic pH is essential for maintaining mast cell secretory granule homeostasis. *Cell death & disease* **8**, e2785, doi:10.1038/cddis.2017.206 (2017).

34 Cipriano, D. J. *et al.* Processive ATP-driven substrate disassembly by the N-ethylmaleimide-sensitive factor (NSF) molecular machine. *The Journal of biological chemistry* **288**, 23436-23445, doi:10.1074/jbc.M113.476705 (2013).

35 Dalal, S., Rosser, M. F. N., Cyr, D. M. & Hanson, P. I. Distinct roles for the AAA ATPases NSF and p97 in the secretory pathway. *Molecular biology of the cell* **15**, 637-648, doi:10.1091/mbc.e03-02-0097 (2004).

36 Deranieh, R. M. *et al.* Perturbation of the Vacuolar ATPase: A NOVEL CONSEQUENCE OF INOSITOL DEPLETION. *The Journal of biological chemistry* **290**, 27460-27472, doi:10.1074/jbc.M115.683706 (2015).

37 Poea-Guyon, S. *et al.* The V-ATPase membrane domain is a sensor of granular pH that controls the exocytotic machinery. *The Journal of cell biology* **203**, 283-298, doi:10.1083/jcb.201303104 (2013).

38 Jena, B. P. Discovery of the Porosome: revealing the molecular mechanism of secretion and membrane fusion in cells. *Journal of cellular and molecular medicine* **8**, 1-21 (2004).

39 Kovari, L. C. *et al.* X-ray solution structure of the native neuronal porosome-synaptic vesicle complex: Implication in neurotransmitter release. *Micron (Oxford, England : 1993)* **56**, 37-43, doi:10.1016/j.micron.2013.10.002 (2014).

40 Wang, S. *et al.* 3D organization and function of the cell: Golgi budding and vesicle biogenesis to docking at the porosome complex. *Histochemistry and cell biology* **137**, 703-718, doi:10.1007/s00418-012-0948-x (2012).

41 Laemmli, U. K. Cleavage of structural proteins during the assembly of the head of bacteriophage T4. *Nature* **227**, 680-685 (1970).

42 Lee, J. S. *et al.* Neuronal porosome proteome: Molecular dynamics and architecture. *Journal of proteomics* **75**, 3952-3962, doi:10.1016/j.jprot.2012.05.017 (2012).

43 Cho, S. J., Wakade, A., Pappas, G. D. & Jena, B. P. New structure involved in transient membrane fusion and exocytosis. *Annals of the New York Academy of Sciences* **971**, 254-256 (2002).

44 Drescher, D. G., Cho, W. J. & Drescher, M. J. Identification of the porosome complex in the hair cell. *Cell biology international reports* **18**, doi:10.1042/cbr20110005 (2011).

45 Deng, Z., Lulevich, V., Liu, F. T. & Liu, G. Y. Applications of atomic force microscopy in biophysical chemistry of cells. *The journal of physical chemistry. B* **114**, 5971-5982, doi:10.1021/jp9114546 (2010).

46 Tsuboi, T. & Rutter, G. A. Insulin secretion by 'kiss-and-run' exocytosis in clonal pancreatic islet beta-cells. *Biochemical Society transactions* **31**, 833-836, doi:10.1042/ (2003).

47 Taraska, J. W., Perrais, D., Ohara-Imaizumi, M., Nagamatsu, S. & Almers, W. Secretory granules are recaptured largely intact after stimulated exocytosis in cultured endocrine cells. *Proceedings of the National Academy of Sciences of the United States of America* **100**, 2070-2075, doi:10.1073/pnas.0337526100 (2003).

48 Aravanis, A. M., Pyle, J. L. & Tsien, R. W. Single synaptic vesicles fusing transiently and successively without loss of identity. *Nature* **423**, 643-647, doi:10.1038/nature01686 (2003).

49 Thorn, P., Fogarty, K. E. & Parker, I. Zymogen granule exocytosis is characterized by long fusion pore openings and preservation of vesicle lipid identity. *Proceedings of the National Academy of Sciences of the United States of America* **101**, 6774-6779, doi:10.1073/pnas.0400336101 (2004).

50 Zimmerberg, J., Cohen, F. S. & Finkelstein, A. Micromolar Ca2+ stimulates fusion of lipid vesicles with planar bilayers containing a calcium-binding protein. *Science (New York, N.Y.)* **210**, 906-908 (1980).

51 Zimmerberg, J., Sardet, C. & Epel, D. Exocytosis of sea urchin egg cortical vesicles *in vitro* is retarded by hyperosmotic sucrose: kinetics of fusion monitored by quantitative light-scattering microscopy. *The Journal of cell biology* **101**, 2398-2410 (1985).

52 Monck, J. R., Oberhauser, A. F., Alvarez de Toledo, G. & Fernandez, J. M. Is swelling of the secretory granule matrix the force that dilates the exocytotic fusion pore? *Biophysical journal* **59**, 39-47, doi:10.1016/s0006-3495(91)82196-8 (1991).

53 Kelly, M. L., Cho, W. J., Jeremic, A., Abu-Hamdah, R. & Jena, B. P. Vesicle swelling regulates content expulsion during secretion. *Cell biology international* **28**, 709-716, doi:10.1016/j.cellbi.2004.07.005 (2004).

54 Sugiya, H., Matsuki-Fukushima, M. & Hashimoto, S. Role of aquaporins and regulation of secretory vesicle volume in cell secretion. *Journal of cellular and molecular medicine* **12**, 1486-1494, doi:10.1111/j.1582-4934.2008.00239.x (2008).

55 Yasui, M., Kwon, T. H., Knepper, M. A., Nielsen, S. & Agre, P. Aquaporin-6: An intracellular vesicle water channel protein in renal epithelia. *Proceedings of the National Academy of Sciences of the United States of America* **96**, 5808-5813, doi:10.1073/pnas.96.10.5808 (1999).

56 Konrad, R. J. *et al.* The heterotrimeric G-protein Gi is localized to the insulin secretory granules of beta-cells and is involved in insulin exocytosis. *The Journal of biological chemistry* **270**, 12869-12876 (1995).

57 Orci, L. *et al.* Conversion of proinsulin to insulin occurs coordinately with acidification of maturing secretory vesicles. *The Journal of cell biology* **103**, 2273-2281 (1986).

58 Orci, L. *et al.* Proteolytic maturation of insulin is a post-Golgi event which occurs in acidifying clathrin-coated secretory vesicles. *Cell* **49**, 865-868 (1987).

59 Rhodes, C. J., Lucas, C. A., Mutkoski, R. L., Orci, L. & Halban, P. A. Stimulation by ATP of proinsulin to insulin conversion in isolated rat pancreatic islet secretory granules. Association with the ATP-dependent proton pump. *The Journal of biological chemistry* **262**, 10712-10717 (1987).

60 Naik, A. R., Kulkarni, S. P., Lewis, K. T., Taatjes, D. J. & Jena, B. P. Functional Reconstitution of the Insulin-Secreting Porosome Complex in Live Cells. *Endocrinology* **157**, 54-60, doi:10.1210/en.2015-1653 (2016).

61 Bradford, M. M. A rapid and sensitive method for the quantitation of microgram quantities of protein utilizing the principle of protein-dye binding. *Analytical biochemistry* **72**, 248-254 (1976).

62 Hettiarachchi, K. D., Zimmet, P. Z. & Myers, M. A. The plecomacrolide vacuolar-ATPase inhibitor bafilomycin, alters insulin signaling in MIN6 beta-cells. *Cell biology and toxicology* **22**, 169-181, doi:10.1007/s10565-006-0054-8 (2006).

63 Weisz, O. A. in *International Review of Cytology* Vol. 226 259-319 (Academic Press, 2003).

64 Hou, J. C., Min, L. & Pessin, J. E. Insulin granule biogenesis, trafficking and exocytosis. *Vitamins and hormones* **80**, 473-506, doi:10.1016/S0083-6729(08)00616-X (2009).

65 Anderson, M., Moshnikova, A., Engelman, D. M., Reshetnyak, Y. K. & Andreev, O. A. Probe for the measurement of cell surface pH *in vivo* and *ex vivo*. *Proceedings of the National Academy of Sciences of the United States of America* **113**, 8177-8181, doi:10.1073/pnas.1608247113 (2016).

66 Berezhnov, A. V. *et al.* Intracellular pH Modulates Autophagy and Mitophagy. *The Journal of biological chemistry* **291**, 8701-8708, doi:10.1074/jbc.M115.691774 (2016).

67 Fang, B., Wang, D., Huang, M., Yu, G. & Li, H. Hypothesis on the relationship between the change in intracellular pH and incidence of sporadic Alzheimer's

disease or vascular dementia. *The International journal of neuroscience* **120**, 591-595, doi:10.3109/00207454.2010.505353 (2010).

68 Robey, I. F. *et al.* Bicarbonate increases tumor pH and inhibits spontaneous metastases. *Cancer research* **69**, 2260-2268, doi:10.1158/0008-5472.can-07-5575 (2009).

69 Bennett, M. K., Calakos, N. & Scheller, R. H. Syntaxin: a synaptic protein implicated in docking of synaptic vesicles at presynaptic active zones. *Science (New York, N.Y.)* **257**, 255-259 (1992).

70 Trimble, W. S., Cowan, D. M. & Scheller, R. H. VAMP-1: a synaptic vesicle-associated integral membrane protein. *Proceedings of the National Academy of Sciences of the United States of America* **85**, 4538-4542, doi:10.1073/pnas.85.12.4538 (1988).

71 Oyler, G. A. *et al.* The identification of a novel synaptosomal-associated protein, SNAP-25, differentially expressed by neuronal subpopulations. *The Journal of cell biology* **109**, 3039-3052, doi:10.1083/jcb.109.6.3039 (1989).

72 Weber, T. *et al.* SNAREpins: minimal machinery for membrane fusion. *Cell* **92**, 759-772 (1998).

73 Cho, S. J. *et al.* SNAREs in opposing bilayers interact in a circular array to form conducting pores. *Biophysical journal* **83**, 2522-2527 (2002).

74 Cho, W. J., Jeremic, A. & Jena, B. P. Size of supramolecular SNARE complex: membrane-directed self-assembly. *Journal of the American Chemical Society* **127**, 10156-10157, doi:10.1021/ja052442m (2005).

75 Jeremic, A., Quinn, A. S., Cho, W. J., Taatjes, D. J. & Jena, B. P. Energy-dependent disassembly of self-assembled SNARE complex: observation at nanometer resolution using atomic force microscopy. *Journal of the American Chemical Society* **128**, 26-27, doi:10.1021/ja056286v (2006).

76 Peters, J. M., Walsh, M. J. & Franke, W. W. An abundant and ubiquitous homo-oligomeric ring-shaped ATPase particle related to the putative vesicle fusion proteins Sec18p and NSF. *The EMBO journal* **9**, 1757-1767 (1990).

77 Tagaya, M., Wilson, D. W., Brunner, M., Arango, N. & Rothman, J. E. Domain structure of an N-ethylmaleimide-sensitive fusion protein involved in vesicular transport. *The Journal of biological chemistry* **268**, 2662-2666 (1993).

78 Matea, C. T. *et al.* Quantum dots in imaging, drug delivery and sensor applications. *International journal of nanomedicine* **12**, 5421-5431, doi:10.2147/IJN.S138624 (2017).

79 Rosenthal, S. J., Chang, J. C., Kovtun, O., McBride, J. R. & Tomlinson, I. D. Biocompatible quantum dots for biological applications. *Chem Biol* **18**, 10-24, doi:10.1016/j.chembiol.2010.11.013 (2011).

80 Jeremic, A. *et al.* Calcium drives fusion of SNARE-apposed bilayers. *Cell biology international* **28**, 19-31, doi:10.1016/j.cellbi.2003.11.004 (2004).

81 Jena, B. P. *et al.* Gi regulation of secretory vesicle swelling examined by atomic force microscopy. *Proceedings of the National Academy of Sciences of the United States of America* **94**, 13317-13322, doi:10.1073/pnas.94.24.13317 (1997).

82 Stokes, G. G. & Royal College of Surgeons of, E. On the effect of the internal friction of fluids on the motion of pendulums. (1851).

83 Gompf, B. & Pecha, R. Mie scattering from a sonoluminescing bubble with high spatial and temporal resolution. *Physical review. E, Statistical physics, plasmas, fluids, and related interdisciplinary topics* **61**, 5253-5256 (2000).

84 Predota, M., Machesky, M. L. & Wesolowski, D. J. Molecular Origins of the Zeta Potential. *Langmuir : the ACS journal of surfaces and colloids* **32**, 10189-10198, doi:10.1021/acs.langmuir.6b02493 (2016).

85 Sun-Wada, G. H. *et al.* The a3 isoform of V-ATPase regulates insulin secretion from pancreatic beta-cells. *Journal of cell science* **119**, 4531-4540, doi:10.1242/jcs.03234 (2006).

86 Fernandes, A. R. & Sa-Correia, I. The activity of plasma membrane H(+)-ATPase is strongly stimulated during Saccharomyces cerevisiae adaptation to growth under high copper stress, accompanying intracellular acidification. *Yeast (Chichester, England)* **18**, 511-521, doi:10.1002/yea.702 (2001).

87 Bertelsen, F. *et al.* Increased GABAA receptor binding in amygdala after prenatal administration of valproic acid to rats. *Acta neuropsychiatrica* **29**, 309-314, doi:10.1017/neu.2016.59 (2017).

88 Kumamaru, E., Egashira, Y., Takenaka, R. & Takamori, S. Valproic acid selectively suppresses the formation of inhibitory synapses in cultured cortical neurons. *Neuroscience letters* **569**, 142-147, doi:10.1016/j.neulet.2014.03.066 (2014).

89 Nalivaeva, N. N., Belyaev, N. D. & Turner, A. J. Sodium valproate: an old drug with new roles. *Trends in pharmacological sciences* **30**, 509-514, doi:10.1016/j.tips.2009.07.002 (2009).

90 Dozawa, M. *et al.* Valproic acid, a histone deacetylase inhibitor, regulates cell proliferation in the adult zebrafish optic tectum. *Developmental dynamics : an official publication of the American Association of Anatomists* **243**, 1401-1415, doi:10.1002/dvdy.24173 (2014).

91 Ganai, S. A., Kalladi, S. M. & Mahadevan, V. HDAC inhibition through valproic acid modulates the methylation profiles in human embryonic kidney cells. *Journal of biomolecular structure & dynamics* **33**, 1185-1197, doi:10.1080/07391102.2014.938247 (2015).

92 Lubrich, B. *et al.* Lithium-induced inositol depletion in rat brain after chronic treatment is restricted to the hypothalamus. *Molecular psychiatry* **2**, 407-412 (1997).

93 Williams, R. S., Cheng, L., Mudge, A. W. & Harwood, A. J. A common mechanism of action for three mood-stabilizing drugs. *Nature* **417**, 292-295, doi:10.1038/417292a (2002).

94 Shaltiel, G. *et al.* Valproate decreases inositol biosynthesis. *Biological psychiatry* **56**, 868-874, doi:10.1016/j.biopsych.2004.08.027 (2004).

95 Teo, R. *et al.* PtdIns(3,4,5)P(3) and inositol depletion as a cellular target of mood stabilizers. *Biochemical Society transactions* **37**, 1110-1114, doi:10.1042/bst0371110 (2009).

96 Berridge, M. J. & Irvine, R. F. Inositol trisphosphate, a novel second messenger in cellular signal transduction. *Nature* **312**, 315-321 (1984).

97 Berridge, M. J. & Irvine, R. F. Inositol phosphates and cell signalling. *Nature* **341**, 197-205, doi:10.1038/341197a0 (1989).

98 Liu, Y. & Bankaitis, V. A. Phosphoinositide phosphatases in cell biology and disease. *Progress in lipid research* **49**, 201-217, doi:10.1016/j.plipres.2009.12.001 (2010).

99 Forgac, M. Vacuolar ATPases: rotary proton pumps in physiology and pathophysiology. *Nature reviews. Molecular cell biology* **8**, 917-929, doi:10.1038/nrm2272 (2007).

100 Brunner, Y. *et al.* Proteomics analysis of insulin secretory granules. *Molecular & cellular proteomics : MCP* **6**, 1007-1017, doi:10.1074/mcp.M600443-MCP200 (2007).

101 Barg, S. *et al.* Priming of insulin granules for exocytosis by granular Cl(-) uptake and acidification. *Journal of cell science* **114**, 2145-2154 (2001).

102 Louagie, E. *et al.* Role of furin in granular acidification in the endocrine pancreas: identification of the V-ATPase subunit Ac45 as a candidate substrate. *Proceedings of the National Academy of Sciences of the United States of America* **105**, 12319-12324, doi:10.1073/pnas.0800340105 (2008).

103 El Far, O. & Seagar, M. A role for V-ATPase subunits in synaptic vesicle fusion? *Journal of neurochemistry* **117**, 603-612, doi:10.1111/j.1471-4159.2011.07234.x (2011).

104 Wang, D. *et al.* Ca2+-Calmodulin regulates SNARE assembly and spontaneous neurotransmitter release via v-ATPase subunit V0a1. *The Journal of cell biology* **205**, 21-31, doi:10.1083/jcb.201312109 (2014).

105 Yu, W., Ye, C. & Greenberg, M. L. Inositol Hexakisphosphate Kinase 1 (IP6K1) Regulates Inositol Synthesis in Mammalian Cells. *The Journal of biological chemistry* **291**, 10437-10444, doi:10.1074/jbc.M116.714816 (2016).

106 Maslanski, J. A., Leshko, L. & Busa, W. B. Lithium-sensitive production of inositol phosphates during amphibian embryonic mesoderm induction. *Science (New York, N.Y.)* **256**, 243-245 (1992).

107 Brodie, M. J. Antiepileptic drug therapy the story so far. *Seizure* **19**, 650-655, doi:10.1016/j.seizure.2010.10.027 (2010).

108 Deranieh, R. M., He, Q., Caruso, J. A. & Greenberg, M. L. Phosphorylation regulates myo-inositol-3-phosphate synthase: a novel regulatory mechanism of inositol biosynthesis. *The Journal of biological chemistry* **288**, 26822-26833, doi:10.1074/jbc.M113.479121 (2013).

109 Tompkins, L. S., Nullmeyer, K. D., Murphy, S. M., Weber, C. S. & Lynch, R. M. Regulation of secretory granule pH in insulin-secreting cells. *American journal of physiology. Cell physiology* **283**, C429-437, doi:10.1152/ajpcell.01066.2000 (2002).

110 Morel, N. & Poea-Guyon, S. The membrane domain of vacuolar H(+)ATPase: a crucial player in neurotransmitter exocytotic release. *Cellular and molecular life sciences : CMLS* **72**, 2561-2573, doi:10.1007/s00018-015-1886-2 (2015).

111 Bodzeta, A., Kahms, M. & Klingauf, J. The Presynaptic v-ATPase Reversibly Disassembles and Thereby Modulates Exocytosis but Is Not Part of the Fusion Machinery. *Cell reports* **20**, 1348-1359, doi:10.1016/j.celrep.2017.07.040 (2017).

112 Di Giovanni, J. *et al.* V-ATPase membrane sector associates with synaptobrevin to modulate neurotransmitter release. *Neuron* **67**, 268-279, doi:10.1016/j.neuron.2010.06.024 (2010).

113 Kane, P. M. The where, when, and how of organelle acidification by the yeast vacuolar H+-ATPase. *Microbiology and molecular biology reviews : MMBR* **70**, 177-191, doi:10.1128/mmbr.70.1.177-191.2006 (2006).

114 Morel, N. Neurotransmitter release: the dark side of the vacuolar-H+ATPase. *Biology of the cell* **95**, 453-457 (2003).

115 Sautin, Y. Y., Lu, M., Gaugler, A., Zhang, L. & Gluck, S. L. Phosphatidylinositol 3-kinase-mediated effects of glucose on vacuolar H+-ATPase assembly, translocation, and acidification of intracellular compartments in renal epithelial cells. *Molecular and cellular biology* **25**, 575-589, doi:10.1128/mcb.25.2.575-589.2005 (2005).

116 Iwata, M. *et al.* Crystal structure of a central stalk subunit C and reversible association/dissociation of vacuole-type ATPase. *Proceedings of the National Academy of Sciences of the United States of America* **101**, 59-64, doi:10.1073/pnas.0305165101 (2004).

ABSTRACT

MOLECULAR MACHINERY FOR THE 'KISS AND RUN' MECHANISM OF INSULIN SECRETION

by

AKSHATA RAMESH NAIK

August 2019

Advisor: Bhanu P. Jena, Ph.D.

Major: Physiology

Degree: Doctor of Philosophy

The insulin secreting porosome is a supramolecular lipo-protein complex that measures roughly 100 – 120 nm in diameter. Porosomes allow transient fusion of insulin secretory granules to the cell plasma membrane and mediates partial release of secretory contents. Post secretion, the secretory granule reseals and re-enters to the cell interior. This is in contrast to the 'total fusion' phenomenon, where secretory vesicles completely fuse at the cell plasma membrane and release all of the contents to the cell exterior. This study involved a deeper understanding of the transient or 'kiss-and-run' mechanism of cell secretion that involves the insulin secreting porosome complex. In addition to the porosome, two other components of transient cell secretion, namely the t/v SNARE complex and the insulin secreting granules (ISGs) were also studied. We demonstrated for the very first time in the history of porosomes, its functional and stable reconstitution into live insulin secreting mouse insulinoma cells leading to improved glucose stimulated insulin releasing from the reconstituted cells. Further, we demonstrated a drop in intracellular pH once a cell has been stimulated for secretion. This lowering of pH is critical for locking in place, the t/v SNARE complex that are present at the base of the porosome.

We also demonstrated a loss in glucose stimulated insulin secretion upon prevention of intracellular acidification utilizing Bafilomycin A, a pharmacological inhibitor of the vacuolar proton pump (vH^+ ATPase). The vH^+ ATPase is also present on the insulin secretory granule membrane, which led to our fourth aim of this study. Valproate, is an FDA approved anticonvulsant that is widely used in the treatment of various neurological disorders such as epilepsy and mood disorders by disturbing vH^+ ATPase activity in the neurons. Since, vH^+ ATPase is also present on ISG membrane we wanted to understand effects of valproate on insulin secretion. We demonstrated that valproate treatment significantly reduces glucose stimulated insulin secretion. Additionally, we also demonstrated that valproate leads to de-localization of one of the cytosolic subunits of vH^+ ATPase from the ISG membrane, preventing complete assembly of the proton pump. These results coherently suggest the importance of porosomes in transient cell secretion and its critical regulation via interaction with various proteins namely SNARE complex and ISG membrane proteins that allows for cell secretion.

AUTOBIOGRAPHICAL SKETCH

AKSHATA RAMESH NAIK

EDUCATION

2019 Ph.D., Wayne State University School of Medicine, Detroit, MI Department of Physiology
2010 M.Sc., University of Mumbai, INDIA, Department of Life Sciences
2008 B.Sc., University of Mumbai, INDIA, Department of Microbiology

PEER REVIEWED PUBLICATIONS

1. Naik, A. R.; Lewis, K. T.; Jena, B. P. The neuronal porosome complex in health and disease. *Experimental biology and medicine (Maywood, N.J.)* **2016,** 241, (2), 115-30. doi: 10.1177/1535370215598400

2. Naik, A. R.; Kulkarni, S. P.; Lewis, K. T.; Taatjes, D. J.; Jena, B. P. Functional Reconstitution of the Insulin-Secreting Porosome Complex in Live Cells. *Endocrinology* **2016,** 157, (1), 54-60. doi: 10.1210/en.2015-1653

3. Arachchige, M. P.; Laha, S. S.; Naik, A. R.; Lewis, K. T.; Naik, R.; Jena, B. P. Functionalized superparamagnetic iron oxide nanoparticles potentiate cellular entry and release of the cancer drug doxorubicin. *Micron (Oxford, England : 1993)* **2017,** 92, 25-31. https://doi.org/10.1016/j.micron.2016.10.005

4. Laha, S. S.; Naik, A. R.; Kuhn, E. R.; Alvarez, M.; Sujkowski, A.; Wessells, R. J.; Jena, B. P. Nanothermometry Measure of Muscle Efficiency. *Nano letters* **2017,** 17, (2), 1262-1268.doi: 10.1021/acs.nanolett.6b05092

5. Lewis, K. T.; Maddipati, K. R.; Naik, A. R.; Jena, B. P. Unique lipid chemistry of synaptic vesicle and synaptosome membrane revealed using mass spectrometry. *ACS chemical neuroscience* **2017,** 8, (6), 1163-1169. doi: 10.1021/acschemneuro.7b00030

6. Lewis, K. T.; Naik, A. R.; Laha, S. S.; Wang, S.; Mao, G.; Kuhn, E.; Jena, B. P. Secretion induces cell pH dyanamics impacting assembly- disassembly of the fusion protein complex: a combined fluorescence and atomic force microscopy study. *Seminars in cell & developmental biology* **2018,** 73, 57-63. doi: 10.1016/j.semcdb.2017.08.003.

7. Yedulla, N. R.; Naik, A. R.; Kokotovich, K. M.; Yu, W.; Greenberg, M. L.; Jena, B. P. Valproate inhibits glucose- stimulated insulin secretion. *Histochemistry and cell biology* **2018,** 150, (4), 395-401. DOI:10.1007/s00418-018-1713-6

8. Kuhn, E. R.; Naik, A. R.; Lewis, B. E.; Kokotovich, K. M.; Li, M.; Stemmler, T. L.; Larsson, L.; Jena, B. P. Nanothermometry reveals calcium-induced remodeling of myosin. *Nano letters* **2018,** 18, (11), 7021-7029. doi: 10.1021/acs.nanolett.8b02989.

9. Naik, A. R.; Pernal, S.; Lewis, K. T.; Wu, Y.; Wu, H.; Carruthers, N. J.; Stemmer, P. M.; Jena, B. P. Human skeletal muscle cells on engineered 3D platform express key growth and developmental proteins. *ACS Biomaterials Science & Engineering* **2019,** 5, (2), 970-976. https://doi.org/10.1021/acsbiomaterials.8b01338

10. Benjamins, J. A.; Nedelkoska, L.; Touil, H.; Stemmer, P. M.; Carruthers, N. J.; Jena, B. P.; Naik, A. R.; Bar-Or, A.; Lisak, R. P. Exosome-enriched fractions from multiple sclerosis B cells induce oligodendrocyte death. *Neurology - Neuroimmunology Neuroinflammation* **2019,** 6, (3), e550. DOI: https://doi.org/10.1212/NXI.0000000000000550.

11. Naik A. R.; Kuhn E.R.; Lewis K. T.; Kokotovich K. M.; Maddipati K. R.; Chen X.; Horber J. H. K.; Taatjes D. J.; Potoff J.; Jena B. P. Self-assembly and biogenesis of cellular membrane is dictated by membrane stretch and composition. *The Journal of Physical Chemistry* **2019**. https://doi.org/10.1021/acs.jpcb.9b04769